Спектроскопия

Спектроскопия 08: Мандельштама - Бриллюэна.

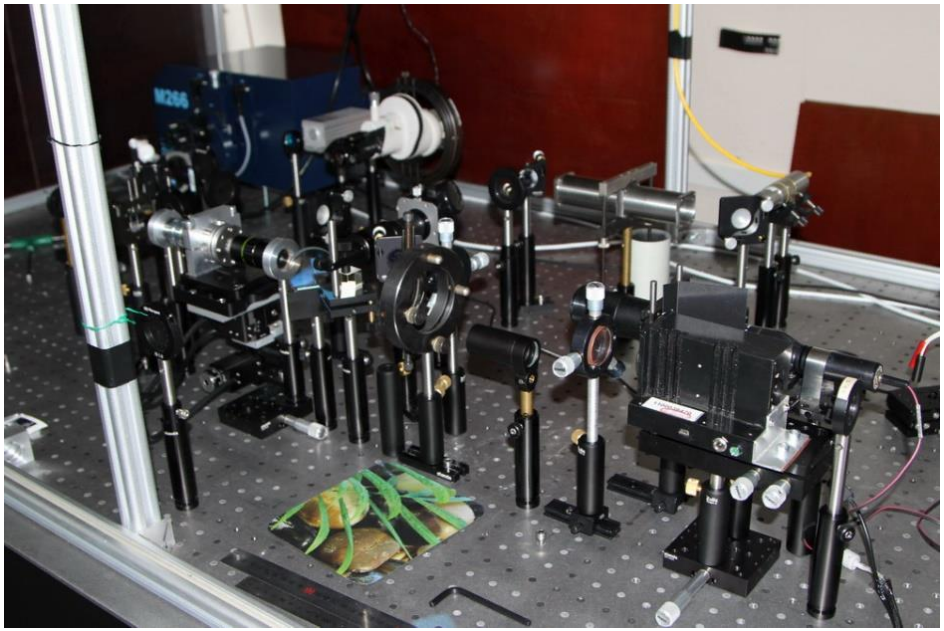

Павел В. Зинин

Why Brillouin Light Scattering (Materials Science)

•As a rule *covalent hard materials* can be obtained under high pressure and high temperature and therefore only in a small amount, usually a few millimeters in size; thus traditional methods for measuring elastic moduli are not applicable. Brillouin scattering has proven to be a unique technique for measuring elastic properties of such small specimens.

•

•The thickness of the *thin films* ranges commonly from a few tens of nanometers up to the order of a micron, and it has been a challenge to characterize the elastic properties of such thin films. Nondestructive methods usually employ surface acoustic waves (SAW), because surface wave displacements are concentrated within a wavelength of the surface and can thus probe the samples within a depth inversely proportional to the frequency used. Surface acoustic wave spectroscopy and acoustic microscopy allow evaluation of elastic properties of the hard films thicker than one micron. For submicron films, frequencies in the range 1 GHz to 50 GHz are needed. The surface Brillouin scattering technique offers the unique opportunity to cover this range of frequencies.

Why Brillouin Light Scattering (Geophysics)

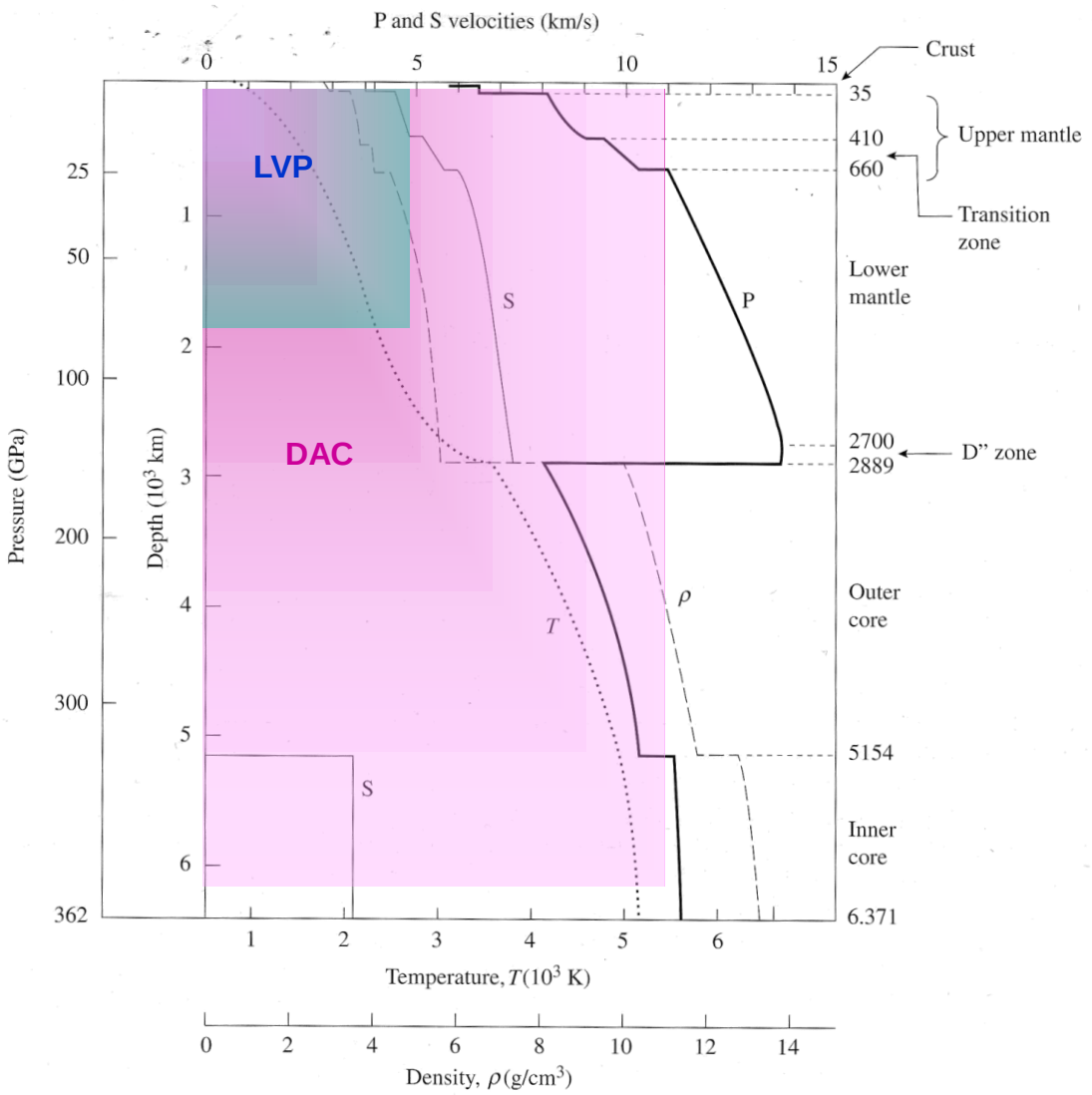

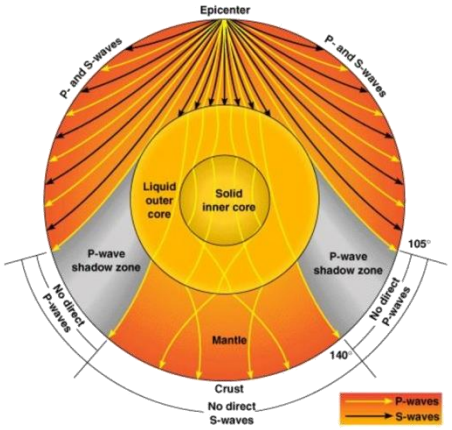

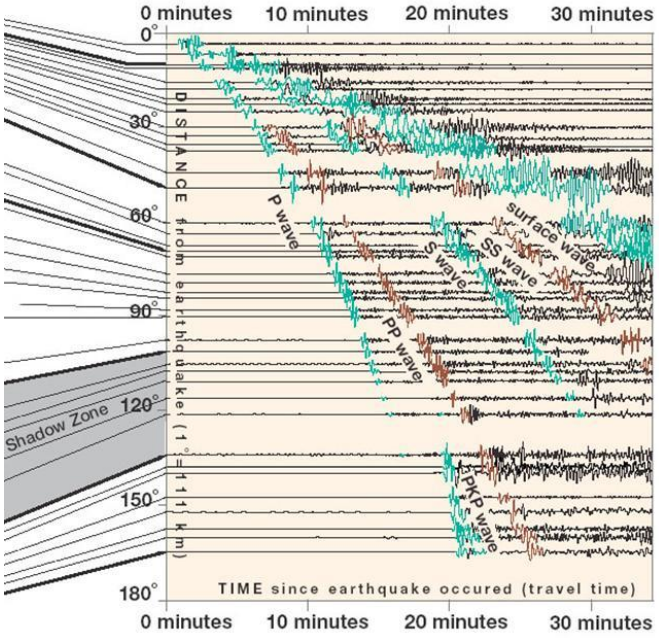

R.Wenk, 2005

Shear Wave Velocity in DAC by Ultrasonic Interferometry

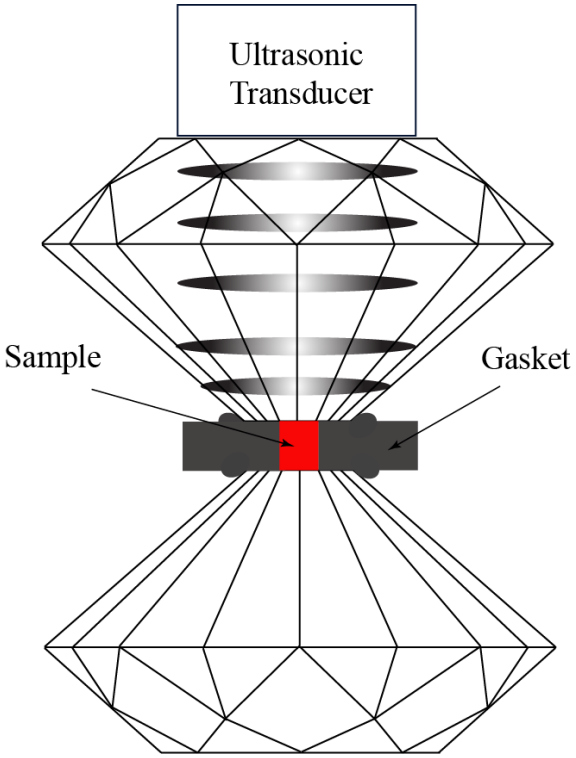

Schematic of acoustical wave propagation in DAC Ultrasonic Interferometry

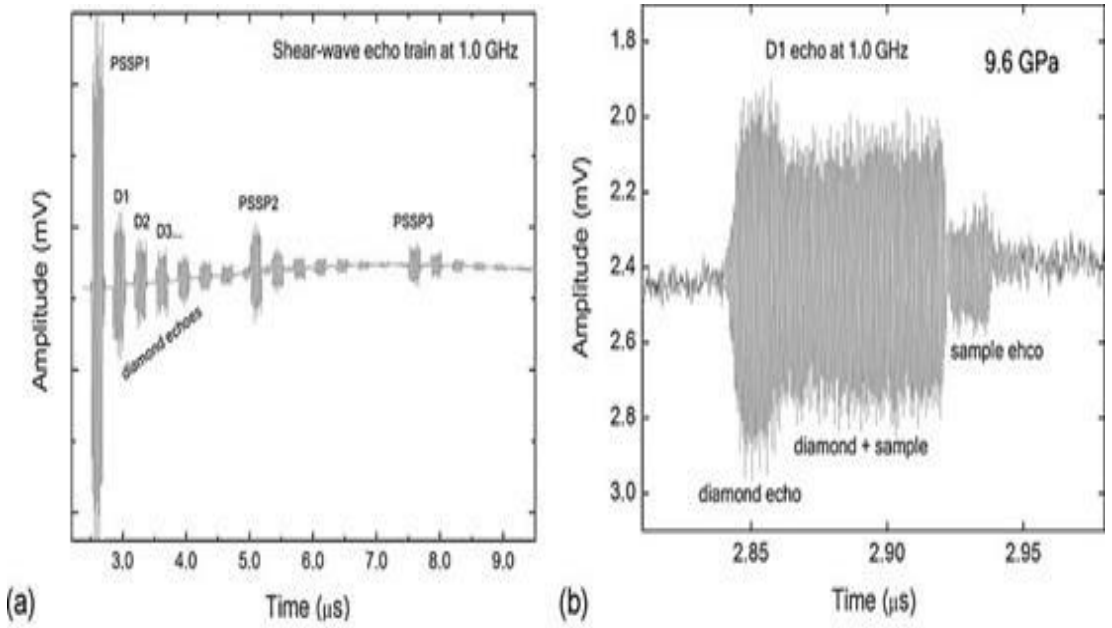

Shear-wave interferometry data from a crystal of $(Mg_{0.22}Fe_{0.78})O$ at 9.6 GPa in the diamond anvil cell. (a) Echo train at 1 GHz showing reflections internal to the buffer rod (labeled PSSP) and multiple S-wave echoes in the diamond (labeled D1, D2, etc.). (b) Expansion of the D1 echo, about 100 ns in duration, reveals the interference between the diamond and sample echoes. The amplitude is measured as a function of frequency at two positions, first before the sample echo arrives (diamond echo) and secondly where there is first-order interference between the diamond and sample.

Мандельштам-Бриллюэнновское рассеяние света

Определение: Мандельштам-Бриллюэн рассеяние (МБР) есть неупругое рассеяние света тепловыми фононами в конденсированной среде.

Предсказание МБР стало возможным благодаря развитию теории тепловых флюктуаций в конденсированной среде в начале 20 века (Смолуховский, Эйнштеин). МБР – рассеяние света на адиабатических флюктуациях плотности конденсированной среды, сопровождающегося изменением частоты.

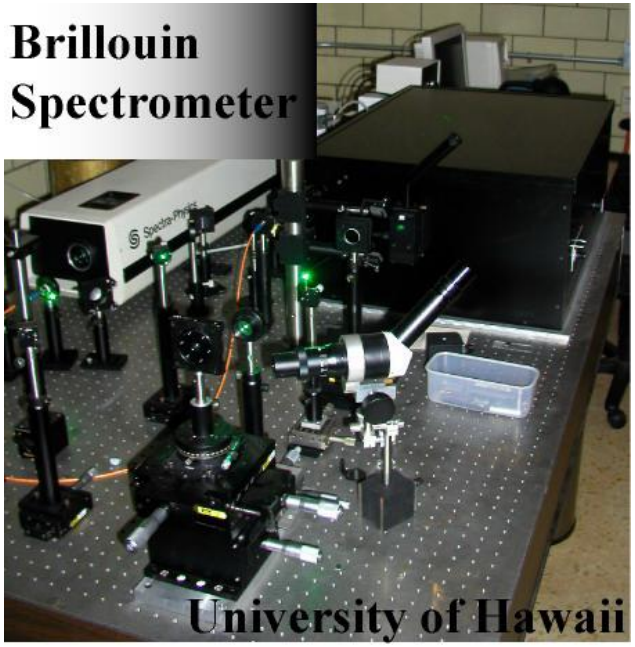

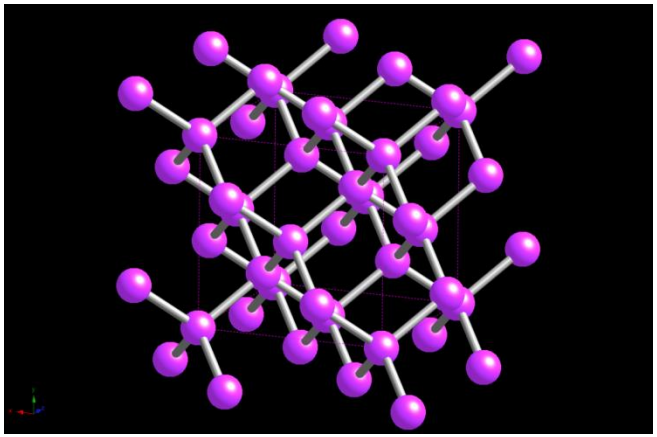

История открытия

Благодаря работам Дебая стало понятным, что тепловые флюктуации плотности могут быть представлены как суперпозиция акустических волн (акустические фононы), распространяющихся вщ всех направлениях в конденсированной среде (L. Landau, E. Lifshits, L. Pitaevskii, *Electrodynamics of Continuous Media*, 1984; Einstein, Ann. Physik, **33**, 1275, 1910).

Первое теоретическое исследование рассеяния света тепловыми фононами было проведено Леонидом Исаковичем Мандельштамом в 1918 году (см. *Фабелинский, 1968; Ландау и др., 1984*), однако соответствующая статья была опубликована только в 1926 году (Мандельштам, Ж. Русь. Физ-Хим. , 58, 381, 1926).

Леон Бриллюэн независимо предсказал рассеяние света от термически возбужденных акустических волн (Brillouin, Ann. Физика. (Paris), 17, 88, 1922).

Обнаружено экспериментально при рассеянии в кристалле кварца и в жидкости Евгением Фёдоровичем Гроссом (1930) и впоследствии им же подробно исследовано (Gross, *Nature*, **126**, 400, 1930).

Leonid Isaakovich Mandelstam

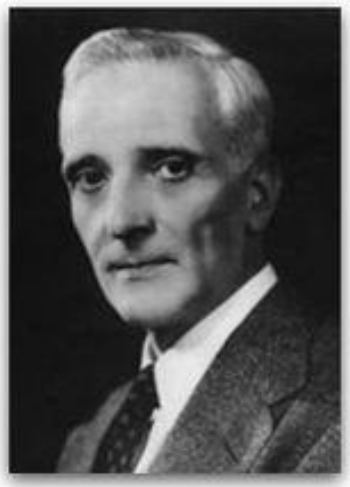

Léon Brillouin

Elasto-optical scattering mechanism: Braggs Law

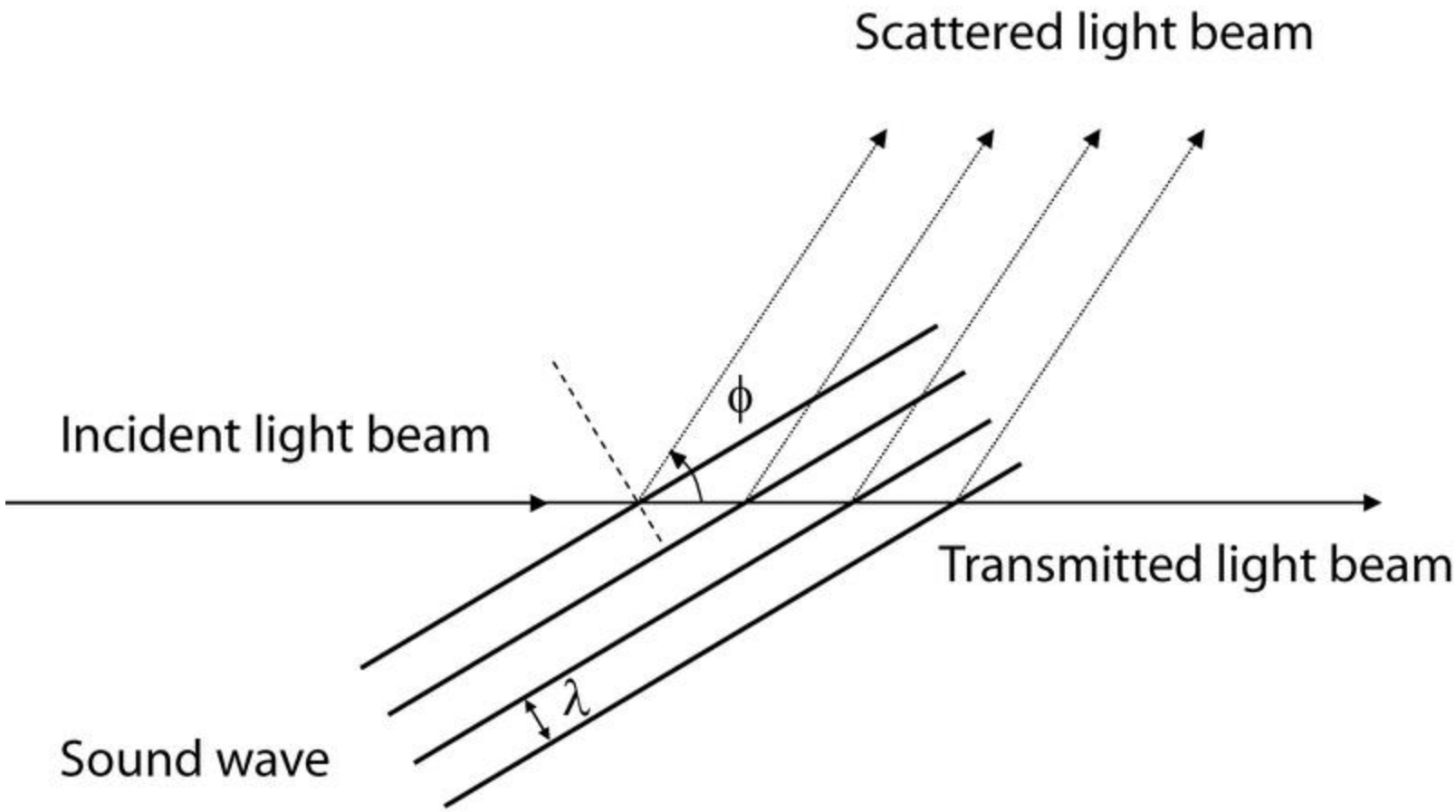

Reflection of Light Waves from Sound Waves

Рассеяние Мандельштама - Бриллюэна

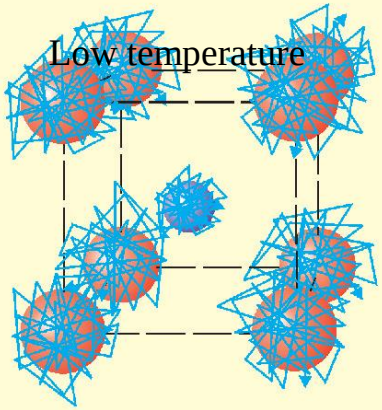

Тепловые колебания атомов

Для лазерного лучу, движущегося в конденсированной среде, тепловые фононы представляют собой движущиеся в всех направления дифракционные решетки. Рассеяние на движущаяся решетка можно наблюдать только в направлениях удовлетворяющих правилу Брэгга-Вольфа. При этом рассеивание происходит с изменением частоты за счет эффекта Доплера, давая рассеянным фотонам сдвинутые частоты Δf.

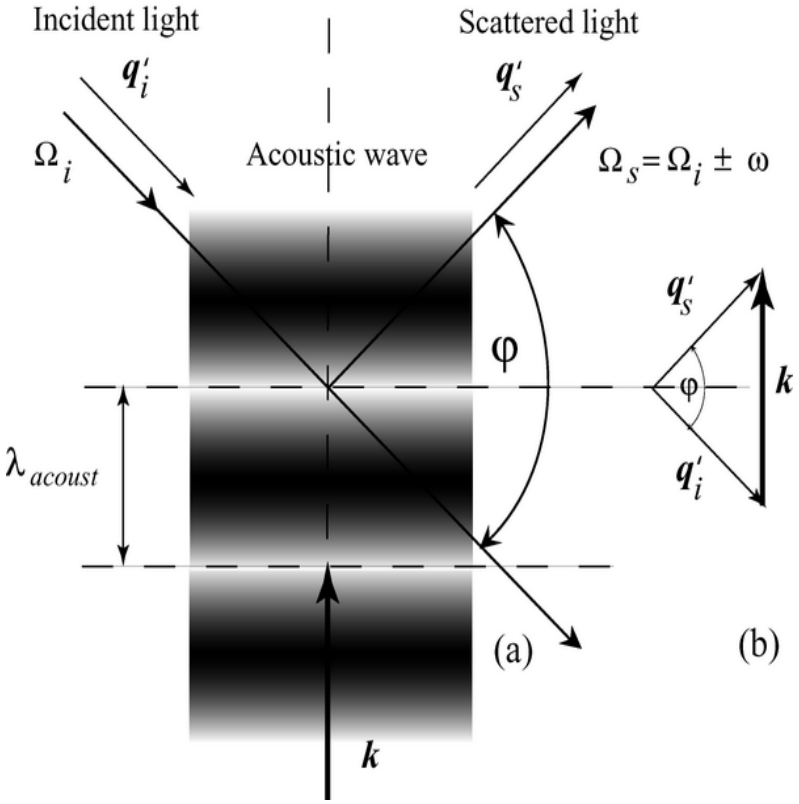

Эскиз светового взаимодействия с акустической волной.

$$V = \frac{\lambda_o \Delta f}{2n \sin\left(\frac{\varphi}{2}\right)}$$

Elasto-optical scattering mechanism

This mechanism occurs as a result of fluctuations in the dielectric constant caused by the phonons moving in thermal equilibrium. It arises from changes in the refractive index produced by the strain generated by sound waves; the change in refractive index is related to the strain through the elasto-optic constants, which determine the degree of interaction between the light and the material. Then, BLS can be viewed as a Bragg's reflection of the incident light wave by the diffraction grating created by thermal phonons. Let φ be the angle between incident and scattered light.

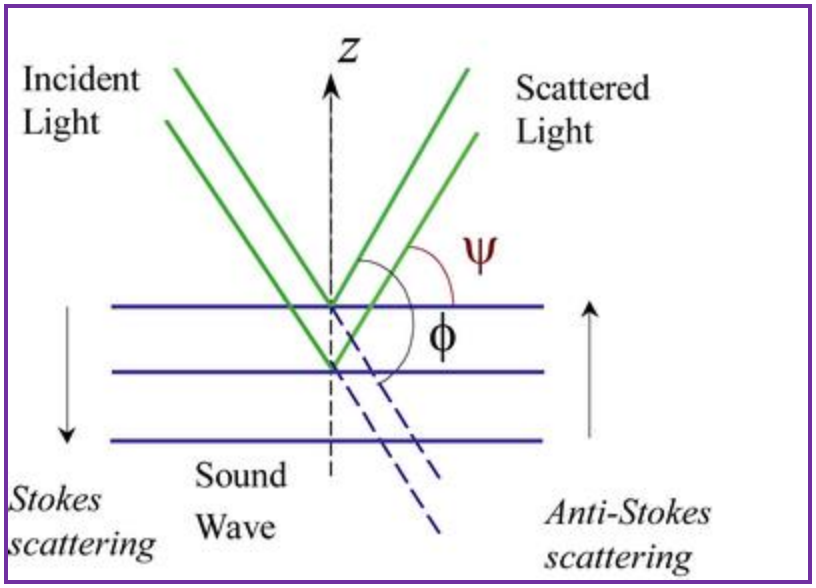

According to the Bragg's law, the grating spacing *d* can be expressed in terms of Bragg's angle ($\psi=\varphi/2$) and wavelength of the laser light inside solid $\lambda = \lambda_o / n$, where λ_o is the laser wavelength in vacuum, and *n* is the index of refraction in the solid

$$2d \sin\psi = 2d \sin\left(\frac{\varphi}{2}\right) = \lambda_o / n$$

Elasto-optical scattering mechanism: Doppler shift

In fact, sound waves are moving through solids and liquids at the speed of sound. As a result of this motion, the light scattered from the sound waves will be shifted up or down in frequency due to the Doppler effect. Scattering from sound waves traveling towards the observer will shift the light up in frequency while scattering from sound waves moving away from the observer will shift it down in frequency. For this reason, the sound wave contribution to Brillouin scattering consists of two peaks shifted up and down from the incident light frequency.

The Doppler shift produces a shift in frequency. When the speed of a moving source or observer, *v*, is much less than the speed of light, the magnitude of the shift in frequency is given to a high degree of precision by the approximate Doppler shift formula:

$$\frac{\Delta f}{f} = \frac{v_{sound}}{c}$$

where Δf is the shift in frequency of the light, f is the original frequency of the light ($\Delta f << f$), v is the velocity of sound, and c is the speed of light.

Elasto-optical scattering mechanism

The moving grating scatters the incident light with a Doppler effect, giving scattered photons shifted frequencies Δf. The Brillouin spectrum gives the frequency shift (Δf) of the thermal phonon, and its wavelength (*d* spacing). The grating space is equal to phonon wave length

$$\frac{2\pi}{|q|} = \frac{V}{\Delta f}$$

Vector ***q*** is the wave vector of the thermal phonon. Then the velocity of the phonon *V* has the form

$$V = \frac{\lambda_o \Delta f}{2n \sin\left(\frac{\varphi}{2}\right)}$$

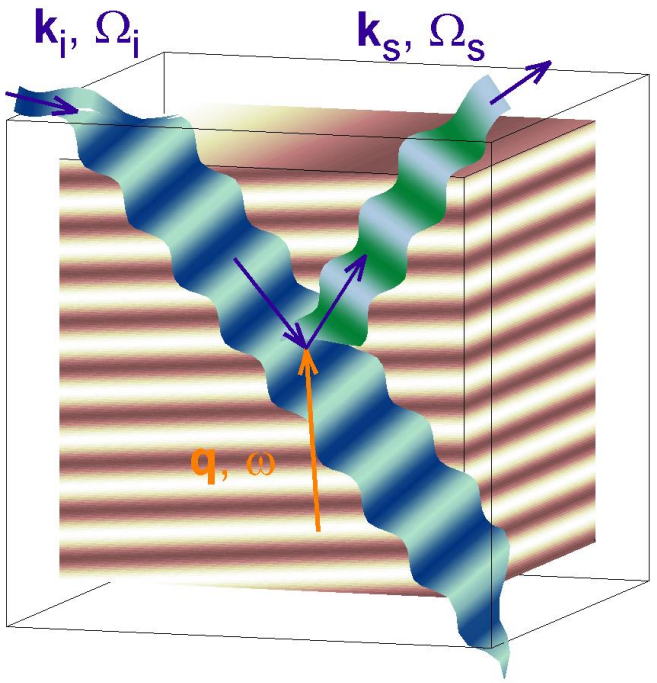

Sketch of the light interaction with acoustic waves (Courtesy to Marco Beghi)

Brillouin Light Scattering (BLS)

Фононы, присутствующие на поверхности образца, движутся в термическом равновесии с очень малыми амплитудами, создавая гофрирование поверхности, которое рассматривается как движущаяся дифракционная решетка падающей световой волной. Поэтому BLS можно объяснить двумя понятиями брэгговского отражения и доплеровского сдвига:

SBS можно рассматривать как Брэгговское отражение падающей волны дифракционной решеткой, созданной тепловыми фононами.
Движущаяся гофрированная поверхность рассеивает падающий свет с эффектом Доплера, давая рассеянные фотоны со смещенными частотами.

BLS может зондировать акустические волны частот до 100 ГГц и характеризовать пленки толщиной до нескольких десятков нанометров.The phonons present at the surface of the sample move in thermal equilibrium with very small amplitudes creating corrugation of the surface, which is viewed as a moving diffraction grating by an incident light wave.

Surface Acoustic Waves

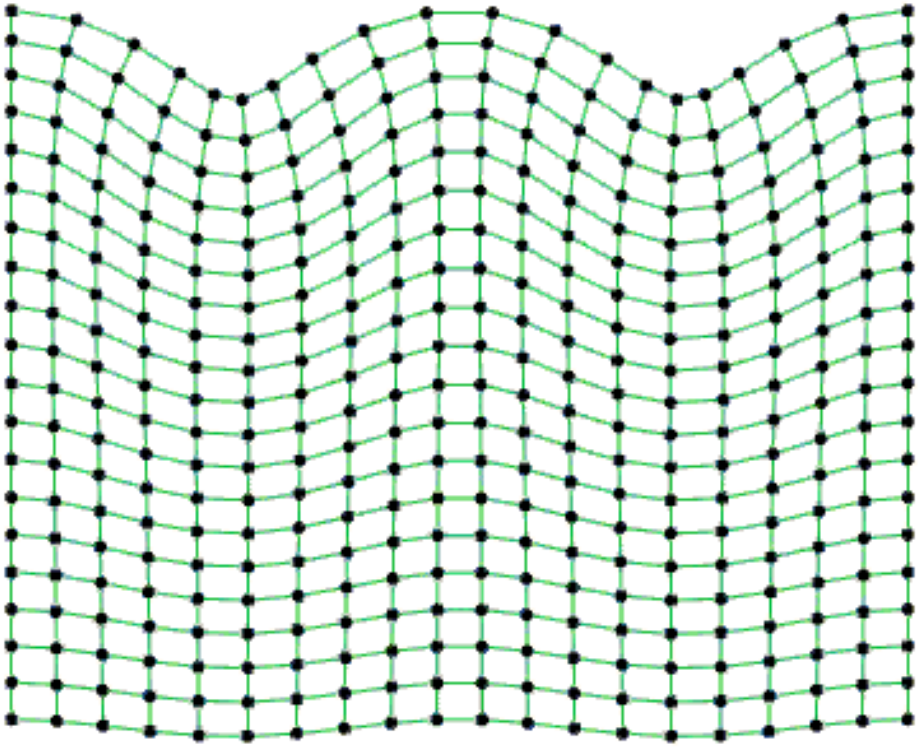

A surface acoustic wave (SAW) is an acoustic wave traveling along the surface of a material exhibiting elasticity, with an amplitude that typically decays exponentially with depth into the substrate (Courtesy to Colm Flannery).

Ripples on the Surface

Surface acoustic waves

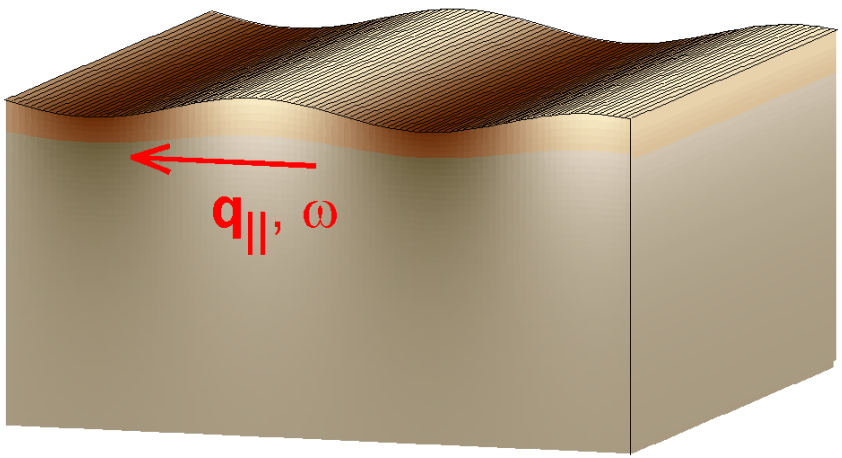

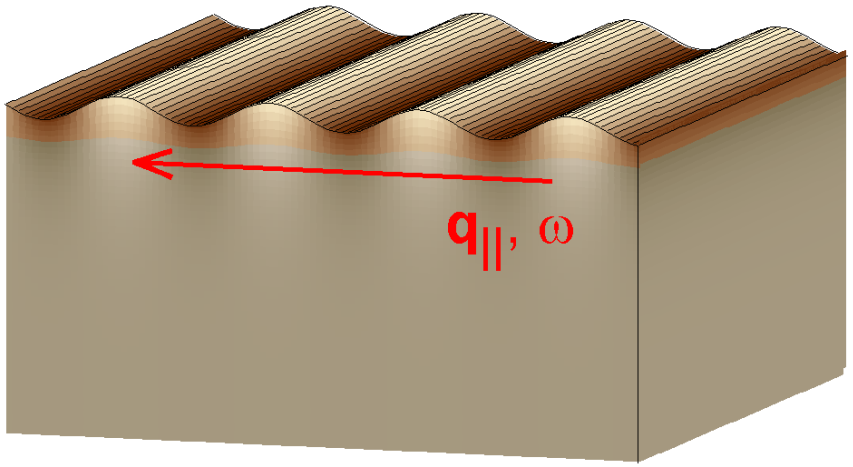

Homogeneous material: $v_{SAW} = v_{SAW}(\rho, C_{ij})$ independent of λ

Layered specimen: v_{SAW} depends on λ and layer geometry

Single layer (thickness h): v_{SAW} depends on $q_{||}h = 2\pi\, h/\lambda$

$q_{||}h << 1$: $v_{SAW} \rightarrow v_{substrate}$

$q_{||}h >> 1$: $v_{SAW} \rightarrow v_{film}$

(Courtesy to Marco Beghi)

Backscattering Configuration

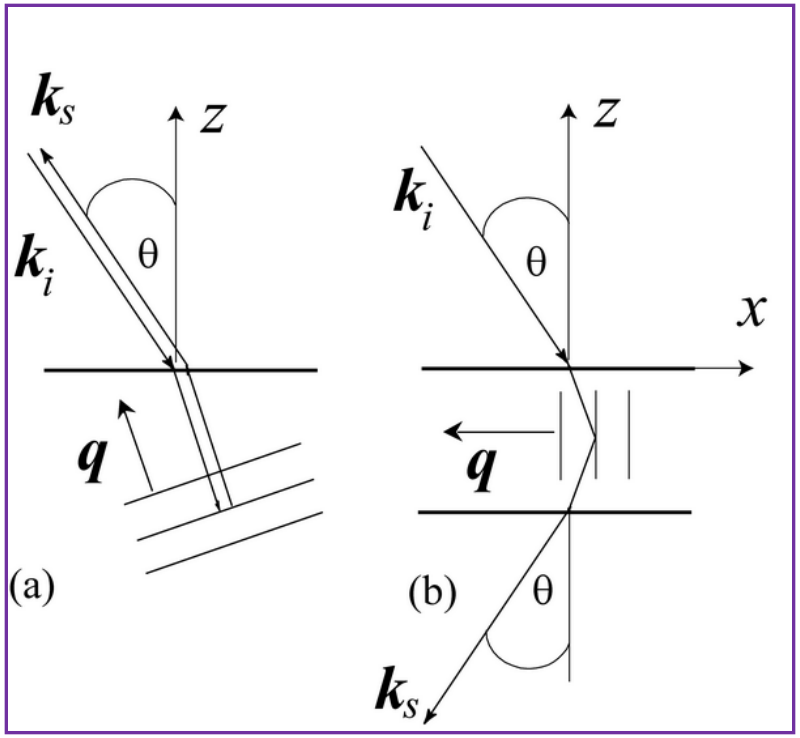

Schematic diagram of the (a) backscattering and (b) platelet configurations. In the platelet configuration Brillouin shift is independent of the refractive index.

Combining the Bragg's law and In the backscattering configuration, light is scattered by thermal phonons propagating parallel to the direction of the incident beam.

$$V = \frac{\lambda_o \delta f}{2n \sin\left(\frac{\varphi}{2}\right)}$$

In the backscattering configuration, light is scattered by thermal phonons propagating parallel to the direction of the incident beam φ=180.

$$V = \frac{\lambda_o \delta f}{2n}$$

Platelet Configuration

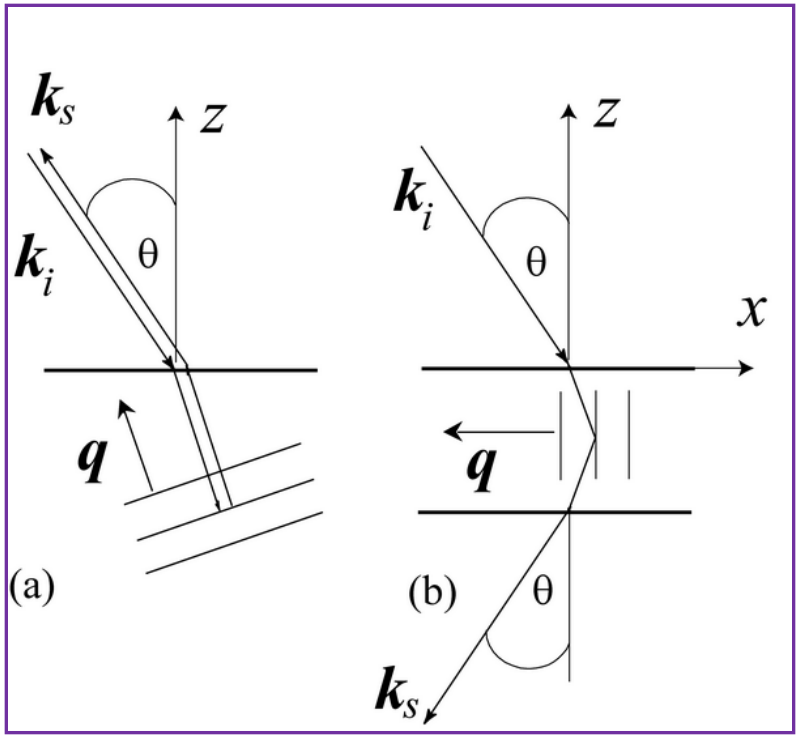

Schematic diagram of the (a) backscattering and (b) platelet configurations. In the platelet configuration Brillouin shift is independent of the refractive index.

In the platelet configuration, light is scattered by thermal phonons propagating parallel to the sample surface. Therefore conditions for ***q*** can be written as

$$q = \pm 2k_x^{'}$$

where is the *x* component of the ***k***i wavevector of the incident light in the medium. According to Snell's law we have

$$k_x^{'} = k_x = \frac{2\pi}{\lambda_o}\sin\theta$$

Combining above equations and the vector momentum and the energy conservation laws we obtain for the platelet configuration

$$V = \frac{\lambda_o \Delta f}{2\sin\theta}$$

“Emulated” platelet configurations

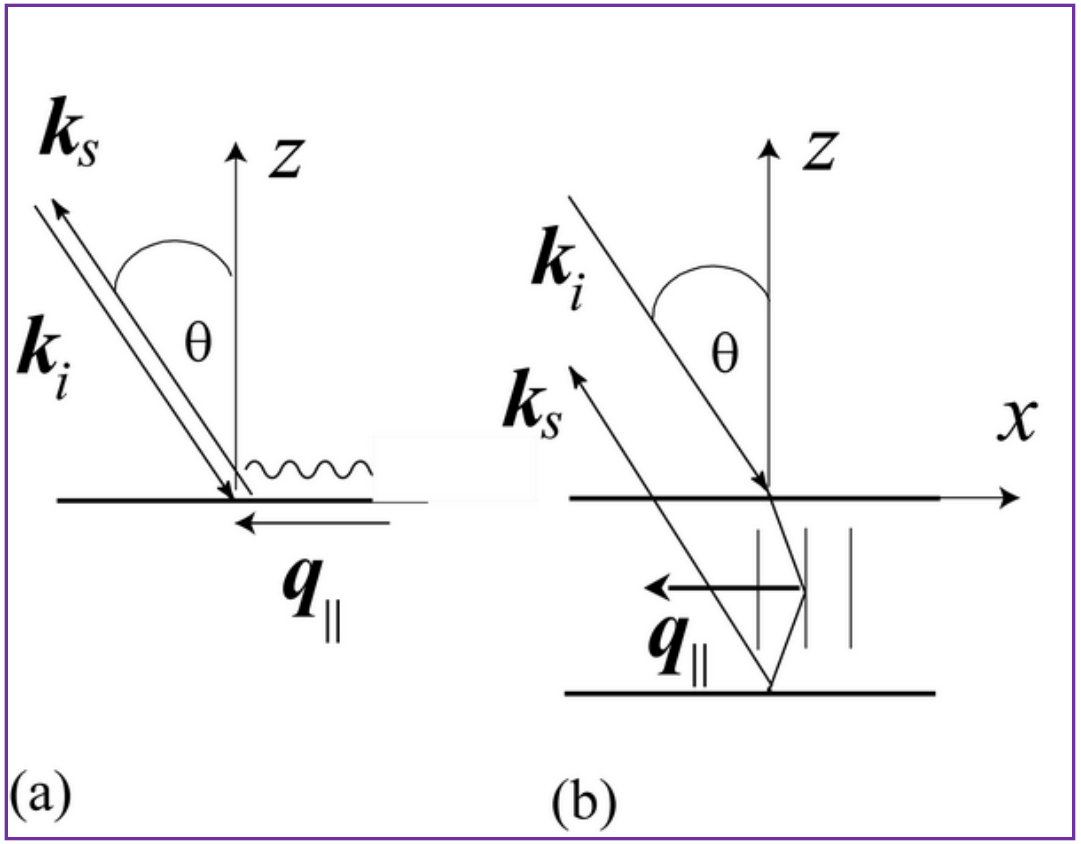

Schematic diagram of the (a) backscattering Surface BLS and (b) “emulated” platelet configurations.

Surface Brillouin Scattering

The phonons present at the surface of the sample move in thermal equilibrium with very small amplitudes creating a corrugation of the surface, which can diffract incident light. The moving corrugated surface scatters the incident light with a Doppler effect, giving scattered photons with shifted frequencies. Equation must thus be redefined because the interaction takes place at the surface and not in the material itself and because continuity now applies to the wavevector component parallel to the surface.

$$\left(\boldsymbol{k}_s - \boldsymbol{k}_i\right)_x = \pm q_{\|} = q$$

Since $k_s \sim k_i$ one can write and in the backscattering mechanism geometry it yields:

$$q_{\|} = \pm 2k\sin\theta$$

Using the vector momentum and the energy conservation laws the surface wave velocity is thus given by

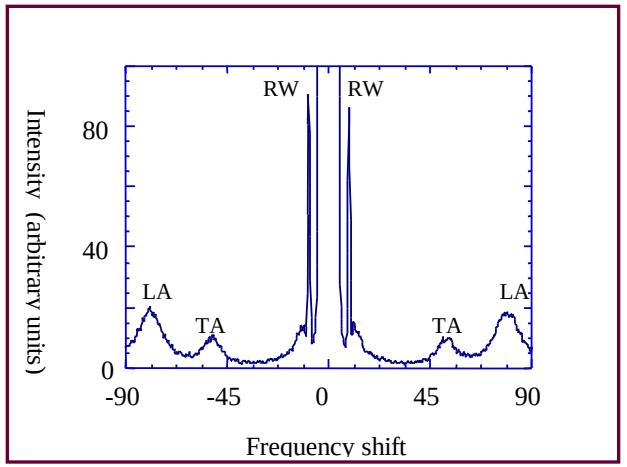

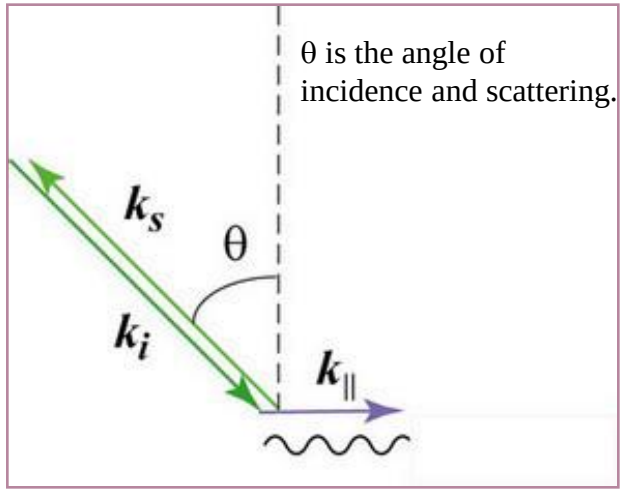

$$V_{SAW} = \frac{\lambda_o \Delta f}{2\sin\theta}$$

Sound Velocity Measurements in DAC: Brillouin scattering

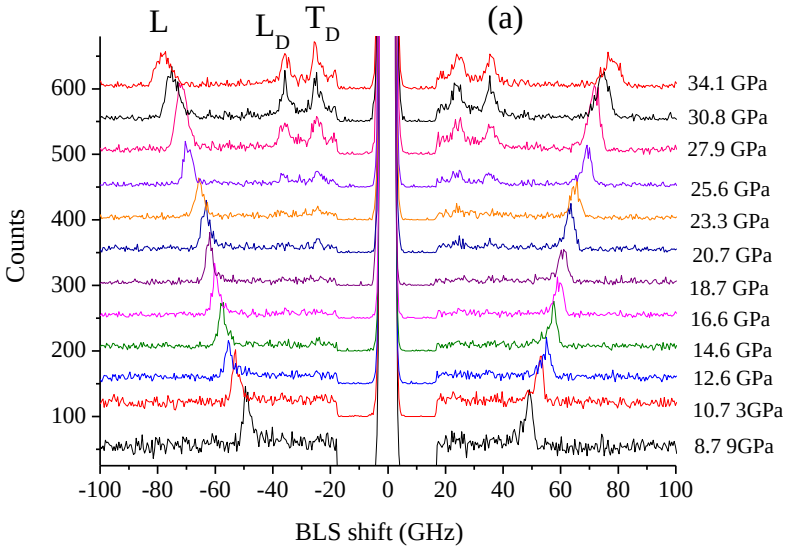

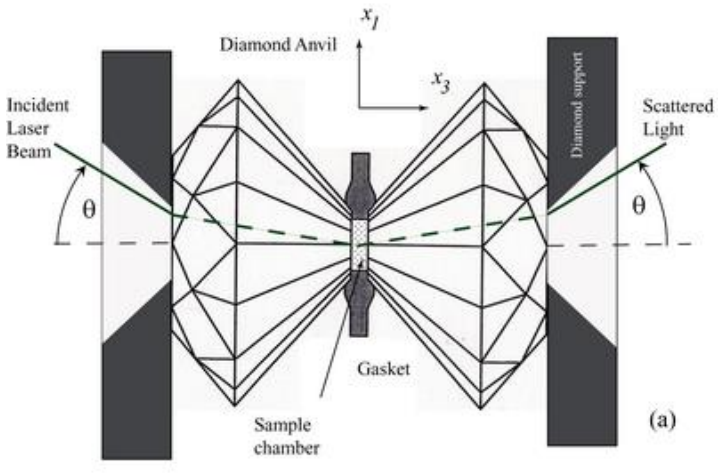

Arrangement for conducting BLS experiments in a DAC

Representative BLS spectra of g-C_3N_4 collected inside a DAC: backscattering configuration.

Then the velocity of the phonon V has the form

$$c_{acoust\_platelet} = \frac{\lambda_o \Delta f}{2 \sin \theta}$$

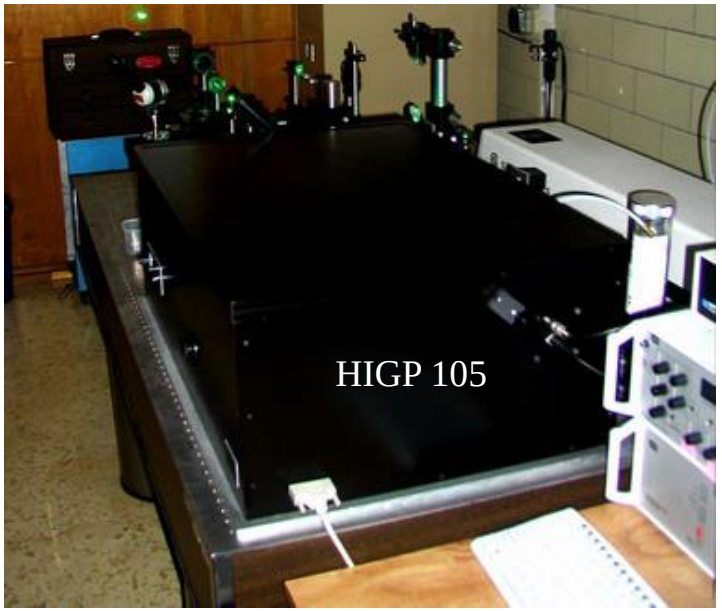

M. G. Beghi, A. G. Every, V. Prakapenka and P. V. Zinin. "Measurements of the Elastic Properties of Solids by Brillouin Spectroscopy", in T. Kundu ed., *Ultrasonic Nondestructive Evaluation: Engineering and Biological Material Characterization*. Taylor & Francis, N.Y., chapter 10, second edition, 540-612 (2012).

Experimental Set-Up

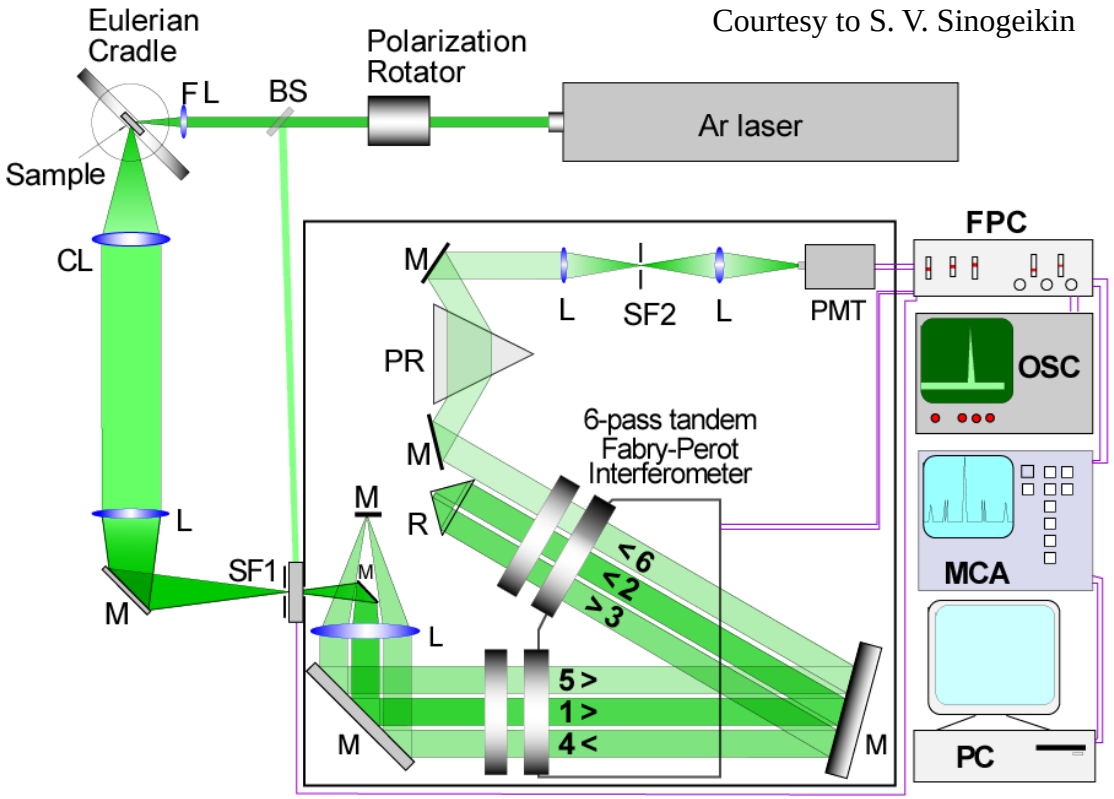

Courtesy to S. V. Sinogeikin

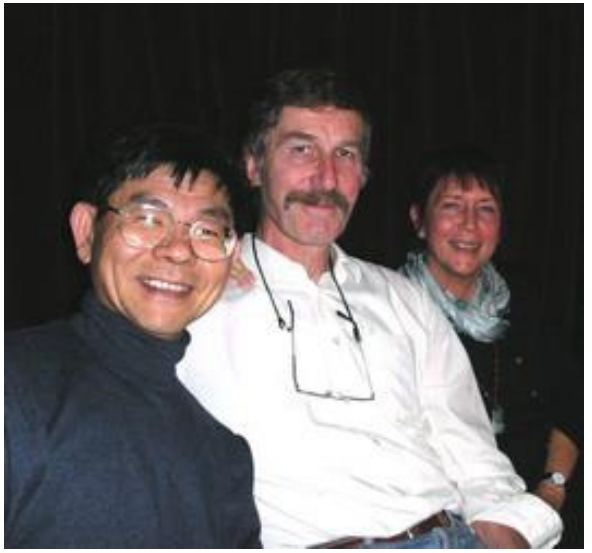

John Sandercock and Li Chung Ming
(Hawaii 2003)

Spectrometer: In almost all Brillouin experiments, the Fabry-Perrot interferometer has been instrument of choice (Grimsditch, 2001). However, conventional Fabry Perot interferometers do not achieve the contrast needed to resolve the weak Brillouin doublets. Sandercock first showed that the contrast can be significantly improved by multipassing (Sandercock, *Opt. Commun*. **2** 73-76 (1970). The usefulness of coupling two synchronized Fabry-Perot, thus avoiding the overlapping of different orders of interference, was also recognized .

Measurements of the elastic properties of BN films

Hexagonal Boron Nitride

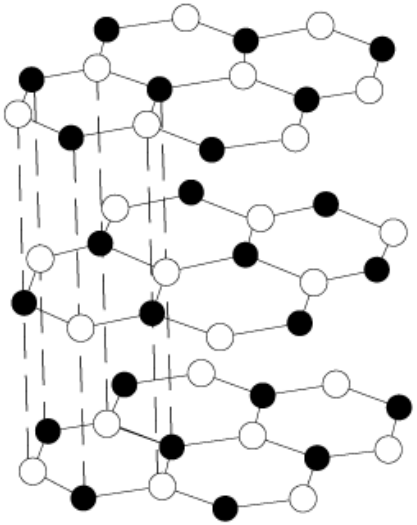

Cubic Boron Nitride

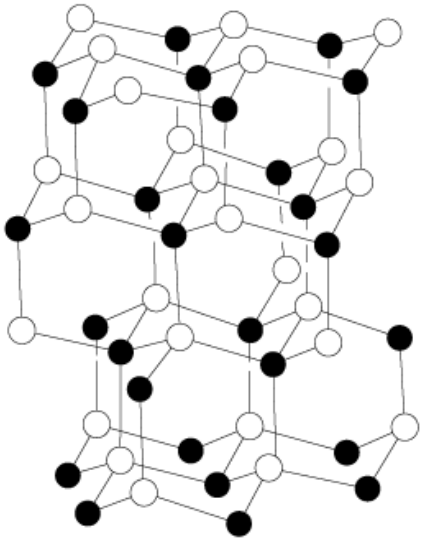

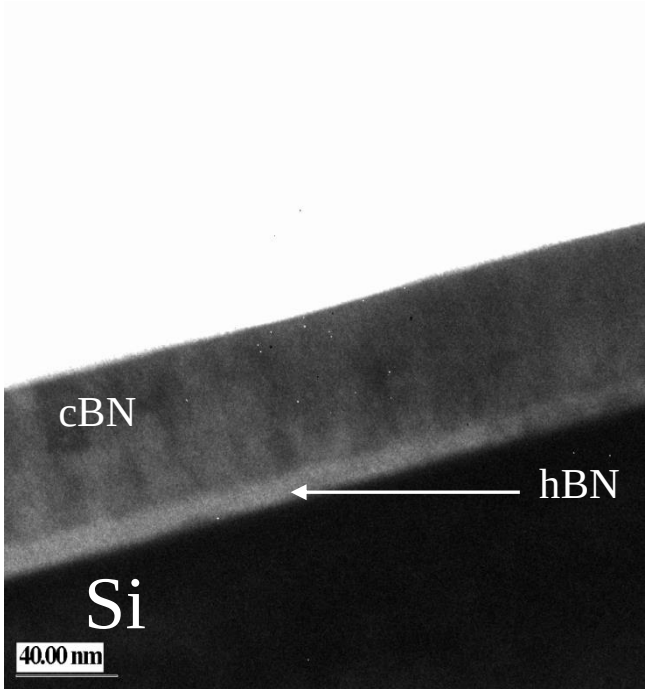

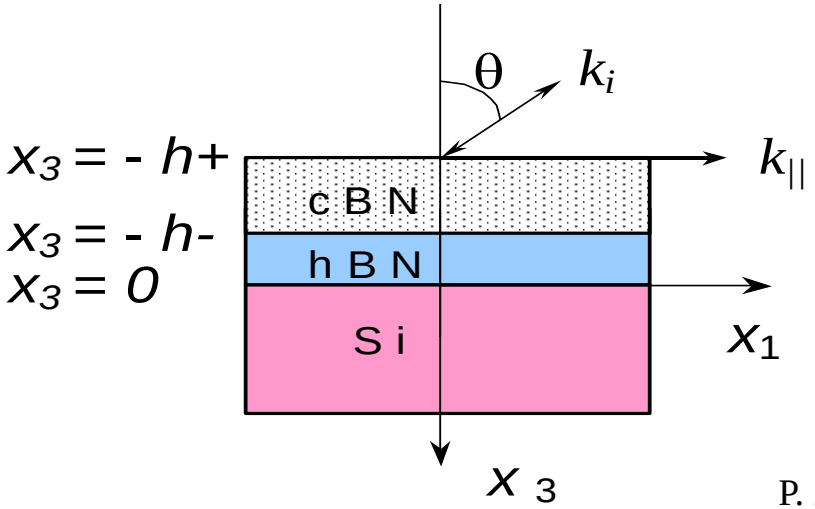

TEM image of cBN (60 nm) /hBN (10 nm) thin film

P. Zinin, M. H. Manghnani, X. Zhang, H. Feldermann, C. Ronning, H. Hofsäss. *J.Appl.Phys.*. **91** 4196 (2002).

Simulated Brillouin spectra of cBN/Si film

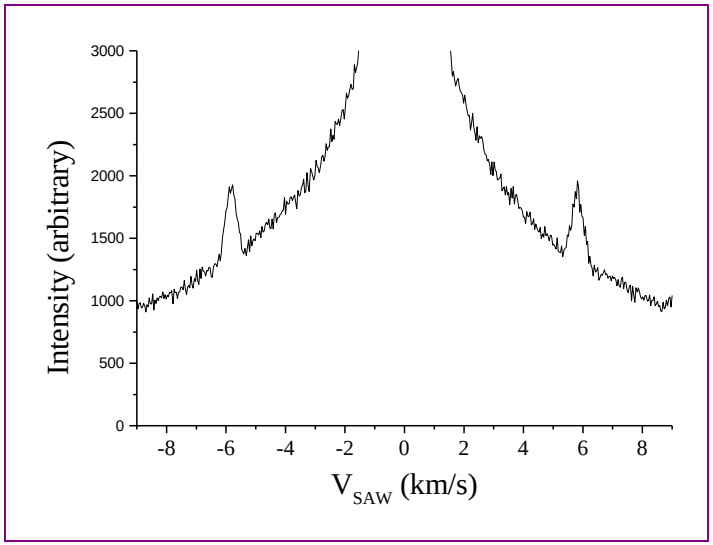

Experimental Brillouin spectrum of cBN/Si film for the angle of 70^{o}.

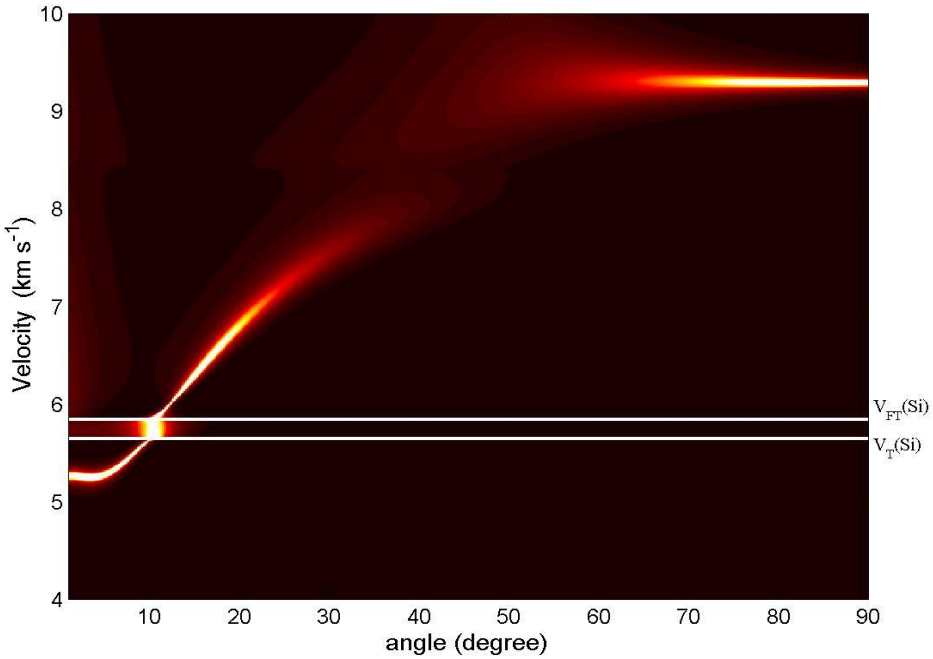

Two-dimensional image of the Brillouin spectra of cBN film (400 nm) on Si (001) calculated for direction [100], using experimentally obtained elastic moduli for cBN. V_T is the transverse-wave threshold; and V_{FT} is the fast transverse threshold.

Dispersion curve for cBN/hBN/Si film

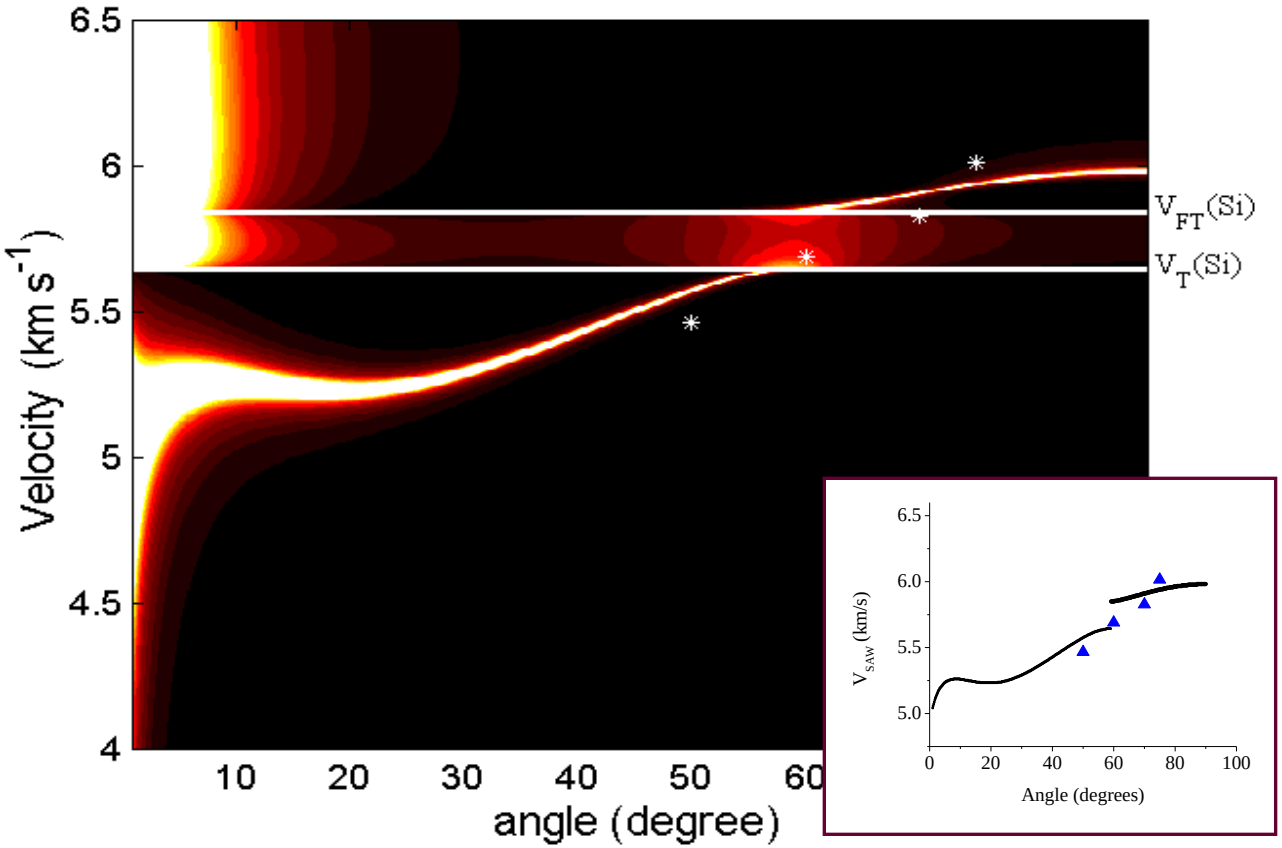

Theoretical SAW dispersion curve for cBN film (60 nm cBN /10 nm hBN) on Si (001) calculated for [100] direction, and compared with experimental data (stars) (Zinin *et al*., JAP. **91** 4196 2002).

Measured and Calculated Moduli of cBN Films

Materials	Density (kg/m3)	C11 (GPa)	C44 (GPa)
*c*BN polycrystalline[a]	3500	876	378
*c*BN isotropic[b]	3500	525	226
*c*BN isotropic[c]		594	266
60 nm *c*BN/10nm *h*BN	3500	875	334

[a] Manghnani, M.H. (1998) *ISAM' 98*.
[b] Wittkowski *et al.* (2000) *Diam. Relat. Mater.*
[c] Pastorelli, R. *et al*. (2000) *Appl. Phys. Lett*.

Emulated Platelet Geometry

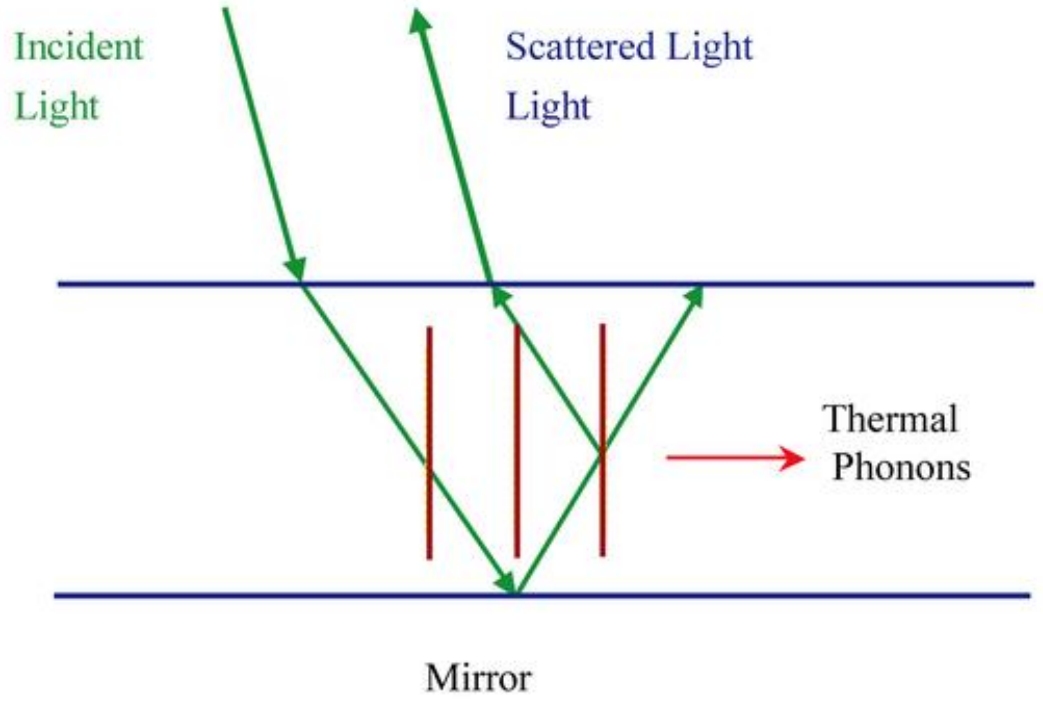

$$V = \frac{\lambda \Delta f}{2 \sin \theta}$$

where θ is the angle between the incident wave vector and normal to the sample surface, and λ is the wave length of the incident light. The advantage of this "modified" geometry enables measurements of the longitudinal (V_L) and transverse (V_T) velocities independent of refractive index n.

Experimental BS spectrum ($\theta = 50^o$) of Nanocrystalline c-BC_2N

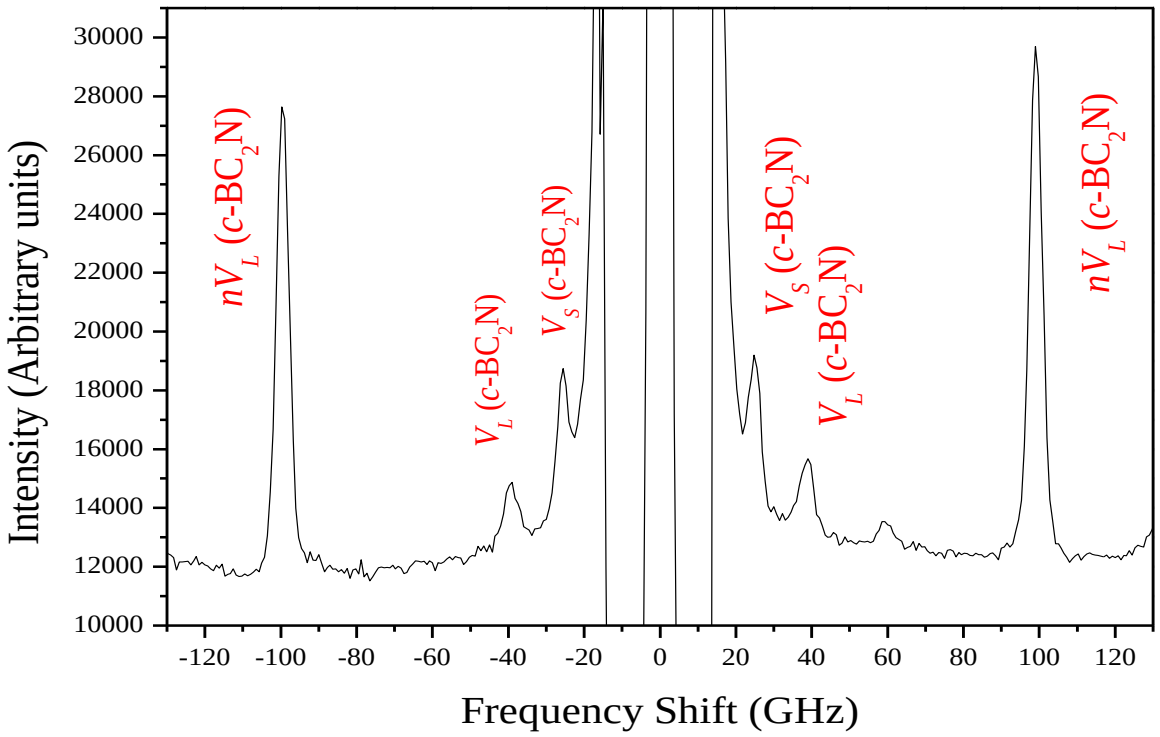

Possible topologically different c-BC2N structures

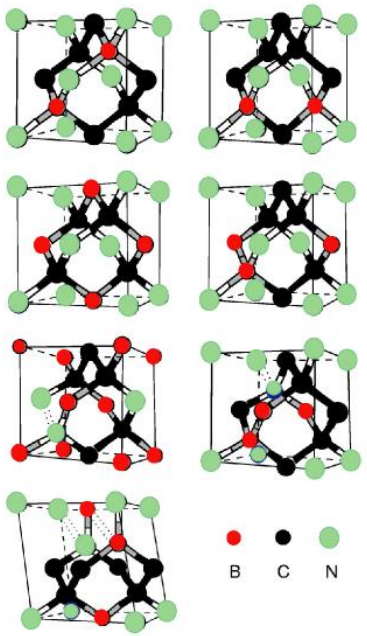

(From Sun et al. PRB 2001)

S. Tkachev, V. Solozhenko, P. Zinin, *et al.*, *Phys. Rev. B.* **68** 052104 (2003).

Summary of experimental data on V_L, V_S, density (ρ) , K, G, and ν of c-BC_2N, cBN and diamond.

Phase	**ρ** (g/cm^3)	**V_L** (km/s)	**V_S** (km/s)	**ν**	**K** (GPa)	**G** (GPa)
Cubic BC_2N	3.358	13.09 ±0.22	8.41 ±0.14	0.149	259 ±22	238±8
cBN	3.500	15.82	10.39	0.121	372.3	377.8
Diamond	3.512	18.17	12.238	0.071	442	538

Elastic moduli and Poisson's ratio of cubic BC_2N were calculated using Brillouin scattering data and value of density was taken from literature. Acoustic velocities and elastic moduli of cBN and diamond were calculated using experimentally measured parameters for single crystals.

Olivine

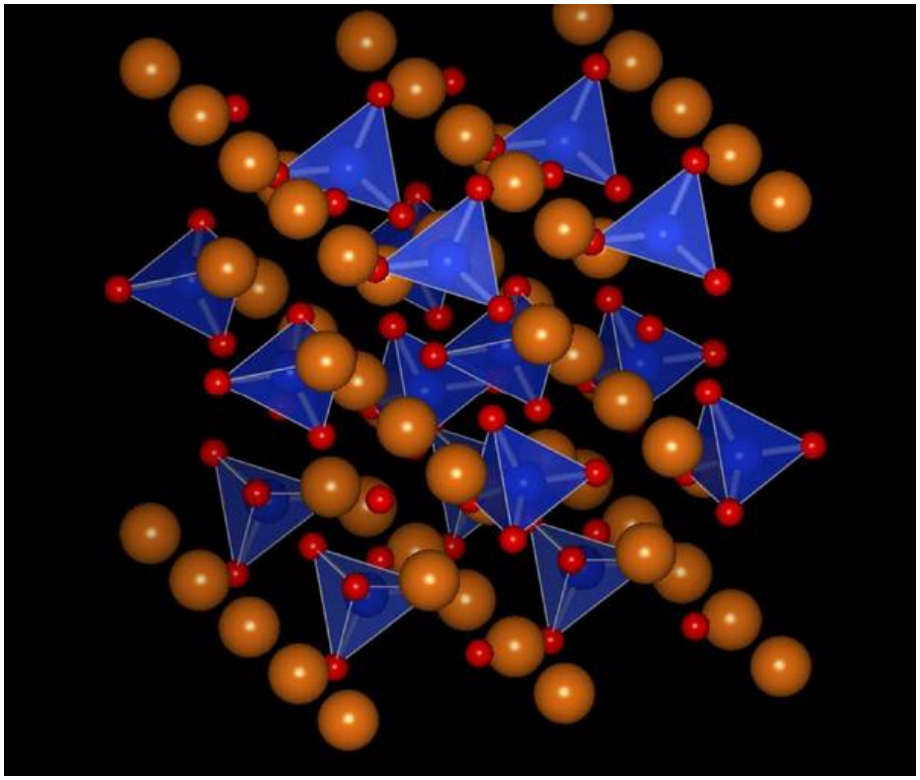

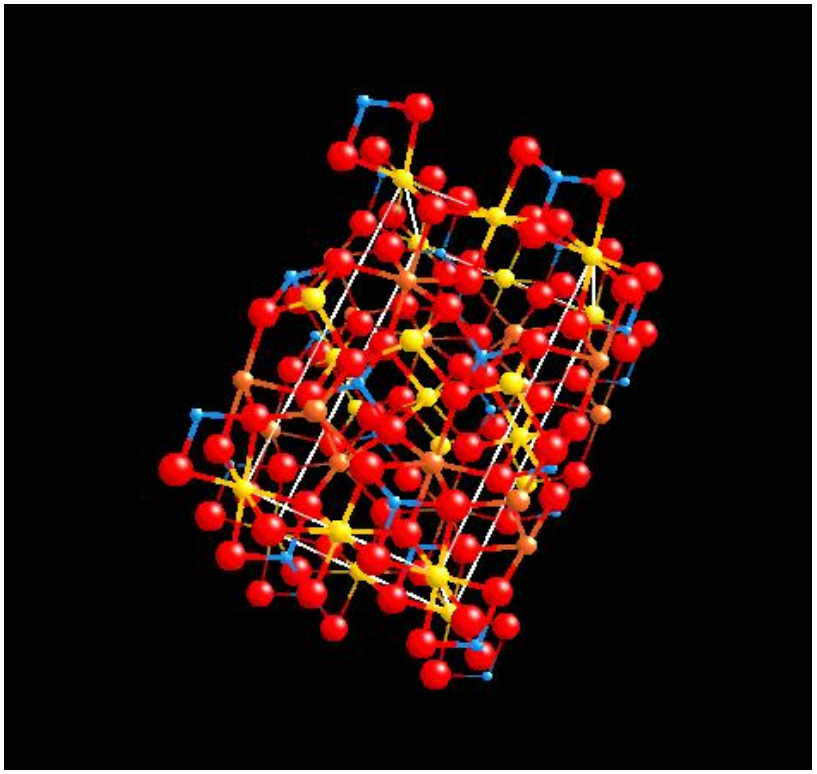

Atomic Structure of Olivine: Mg_2SiO_4
(Symmetry: Orthorhombic: a:b:c =0.4648:1:0.5857)

Anisotropic Elasticity: Stress-strain relation

The relation between stress and strain in general is described by the tensor of elastic constants c_{ijkl}

$$\sigma_{ij} = c_{ijkl}\varepsilon_{kl}$$

Generalised Hooke's Law

From the symmetry of the stress and strain tensor and a thermodynamic condition if follows that the maximum number if independent constants of c_{ijkl} is 21. In an isotropic body, where the properties do not depend on direction the relation reduces to

$$\sigma_{ij} = \lambda\Theta\delta_{ij} + 2\mu\varepsilon_{ij}$$

Hooke's Law

where l and m are the Lame parameters, q is the dilatation and d_{ij} is the Kronecker delta.

$$\Theta\delta_{ij} = \varepsilon_{kk}\delta_{ij} = \left(\varepsilon_{xx} + \varepsilon_{yy} + \varepsilon_{zz}\right)\delta_{ij}$$

Anisotropic Elasticity: Stress-strain relation

$$\sigma_{ij} = c_{ijkl}\varepsilon_{kl}$$

$$\varepsilon_{ik} = \frac{1}{2}\left(\frac{\partial u_i}{\partial x_k} + \frac{\partial u_k}{\partial x_i}\right)$$

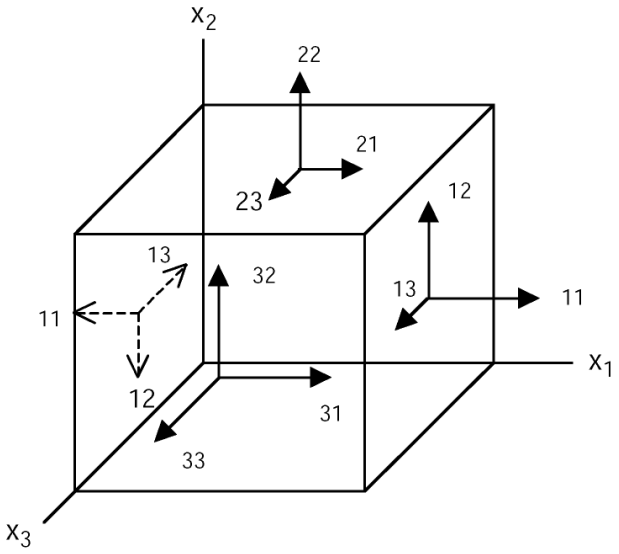

Different stress components in $x_1x_2x_3$ coordinate system

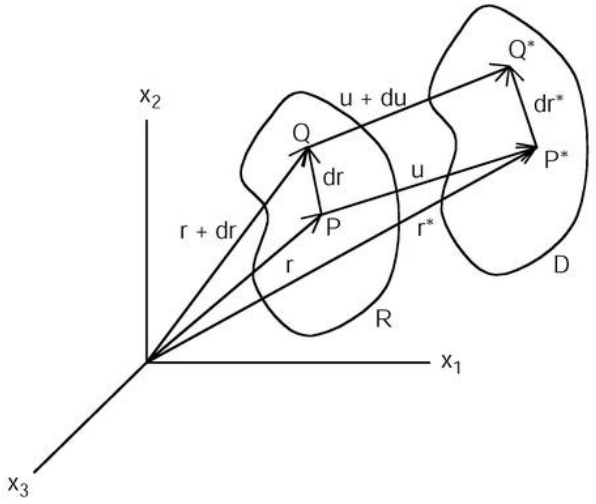

Deformation of a body. R is the reference state, and D is the deformed state.

Position vectors of P, Q, P , and Q * are **r, r+dr, r* and r+dr***, respectively

Anisotropic Elasticity

For anisotropic materials, the stress-strain relation of can be written in the following form:

$$\begin{Bmatrix} \sigma_{11} \\ \sigma_{22} \\ \sigma_{33} \\ \sigma_{23} \\ \sigma_{31} \\ \sigma_{12} \end{Bmatrix} = \begin{Bmatrix} C_{1111} & C_{1122} & C_{1133} & C_{1123} & C_{1132} & C_{1112} \\ C_{2211} & C_{2222} & C_{2223} & C_{2223} & C_{2232} & C_{2212} \\ C_{3311} & C_{3322} & C_{3333} & C_{3323} & C_{3332} & C_{3312} \\ C_{2311} & C_{2322} & C_{2333} & C_{2323} & C_{2332} & C_{2312} \\ C_{3111} & C_{3122} & C_{3133} & C_{3123} & C_{3132} & C_{3112} \\ C_{1211} & C_{1222} & C_{1233} & C_{1223} & C_{1232} & C_{1212} \end{Bmatrix} \begin{Bmatrix} \varepsilon_{11} \\ \varepsilon_{22} \\ \varepsilon_{33} \\ \varepsilon_{23} \\ \varepsilon_{31} \\ \varepsilon_{12} \end{Bmatrix}$$

the coefficient values *Cijkl* depend on the material type and are called material constants or elastic constants

Anisotropic Elasticity

For anisotropic media, the elasticity tensor C_{ijkl} is more complicated, and in fact cannot even be depicted compactly on paper or screen, because of the four subscripts. Fortunately, the symmetry of the stress tensor σ_{ij} means that there are at most 6 different elements of stress. Similarly, there are at most 6 different elements of the strain tensor ε_{ij}. Hence the 4th rank elasticity C_{ijkl} tensor may be written as a 2nd rank matrix $C_{\alpha\beta}$. Voigt notation is the standard mapping for tensor indices,

ij	=	11	22	33	23,32	13,31	12,21
⇓		⇓	⇓	⇓	⇓	⇓	⇓
α	=	1	2	3	4	5	6

With this notation, one can write the elasticity matrix for any linearly elastic medium as: and are called material constants or elastic constants

$$\begin{Bmatrix} \sigma_{11} \\ \sigma_{22} \\ \sigma_{33} \\ \sigma_{23} \\ \sigma_{31} \\ \sigma_{12} \end{Bmatrix} = \begin{Bmatrix} C_{11} & C_{12} & C_{13} & C_{14} & C_{15} & C_{16} \\ C_{12} & C_{22} & C_{23} & C_{24} & C_{25} & C_{26} \\ C_{13} & C_{23} & C_{33} & C_{34} & C_{35} & C_{36} \\ C_{14} & C_{24} & C_{34} & C_{44} & C_{45} & C_{56} \\ C_{15} & C_{25} & C_{35} & C_{45} & C_{55} & C_{56} \\ C_{16} & C_{26} & C_{36} & C_{46} & C_{56} & C_{66} \end{Bmatrix} \begin{Bmatrix} \varepsilon_1 \\ \varepsilon_2 \\ \varepsilon_3 \\ \varepsilon_2 \\ \varepsilon_3 \\ \varepsilon_1 \end{Bmatrix}$$

Isotropic and Cubic Crystals

As shown, the matrix $C_{\alpha\beta}$ is symmetric, because of the linear relation between stress and strain. Hence, there are at most 21 different elements of $C_{\alpha\beta}$. The isotropic special case has 2 independent elements:

C_{11}	C_{12}	C_{12}	0	0	0
	C_{11}	C_{12}	0	0	0
		C_{11}	0	0	0
			$0.5(C_{11}-C_{12})$	0	0
				$0.5(C_{11}-C_{12})$	
					$0.5(C_{11}-C_{12})$

Materials with cubic symmetry has 3 independent elements:

C_{11}	C_{12}	C_{12}	0	0	0
C_{12}	C_{11}	C_{12}	0	0	0
C_{12}	C_{12}	C_{11}	0	0	0
0	0	0	C_{44}	0	0
0	0	0	0	C_{44}	9
0	0	0	0	0	C_{44}

Hexagonal symmetry

Materials with hexagonal elastic symmetry has 5 independent elements:

C_{11}	C_{12}	C_{13}	0	0	0
C_{12}	C_{11}	C_{13}	0	0	0
C_{13}	C_{13}	C_{33}	0	0	0
0	0	0	C_{44}	0	0
0	0	0	0	C_{44}	
0	0	0	0	0	$0.5(C_{11}-C_{12})$

The trigonal crystal has 5 independent constants, orthorombic crystal has 9 independent constants, monoclinic crystal has 13 independent constants and triclinic crystal has 21 independent constants.

Section through oxide film

Acoustic Waves in Anisotropic Solids

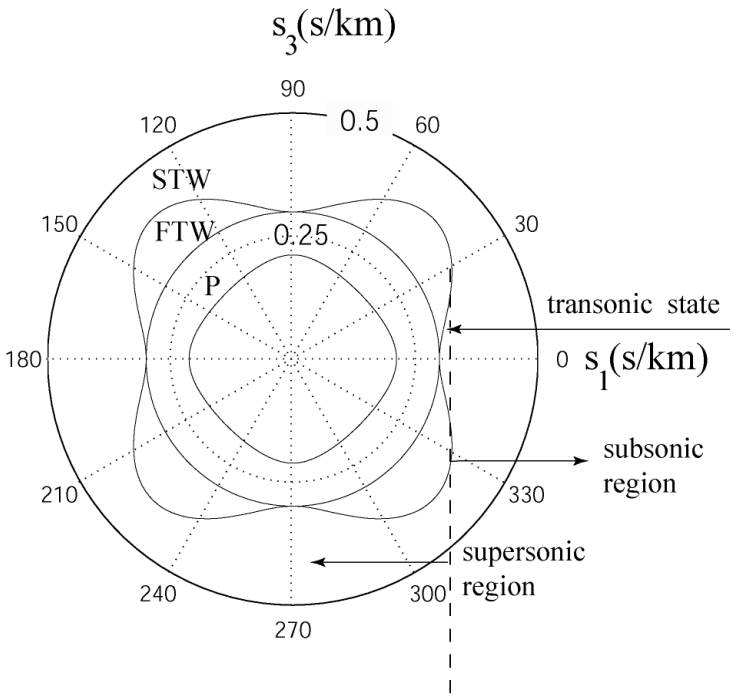

The slowness curve of silicon for the (001) plane. The dashed line corresponds the transonic state. The solid curves correspond the slowness curves for longitudinal P, FT and ST bulk waves.

In isotropic solids two types of bulk acoustic modes exist: primary waves, longitudinally polarized, and secondary waves, transversely polarized. Two independent (orthogonal) transverse polarization directions exist. In isotropic solids the secondary waves are perfectly equivalent, while in anisotropic solids they are not. These modes, called fast transverse (FT) and slow transverse (ST) from their generally different velocities, have phase velocities and polarization vectors which depend on the propagation direction. Also the phase velocity and polarization vector of the longitudinal (P) mode depend on the propagation direction.

Single-crystal and aggregate elastic properties

- In general acoustic *velocities* in crystals vary with crystallographic *direction*.
- Velocity measurements in more than one direction are needed to completely characterize the elasticity / velocity of elastically anisotropic crystals.
- From acoustic velocities as a function of crystallographic *direction* can calculate single-crystal elastic *moduli* (C_{ij}), which completely characterize the elasticity of a material.
- e.g. $C_{11} = \rho V^2_{P(100)}$
- $\left| C_{ijkl} a_j a_l - \rho V^2 \delta_{ik} \right| = 0$
- From single-crystal elastic bulk (K) and shear (μ) *moduli*, as well as aggregate acoustic velocities are readily calculated.

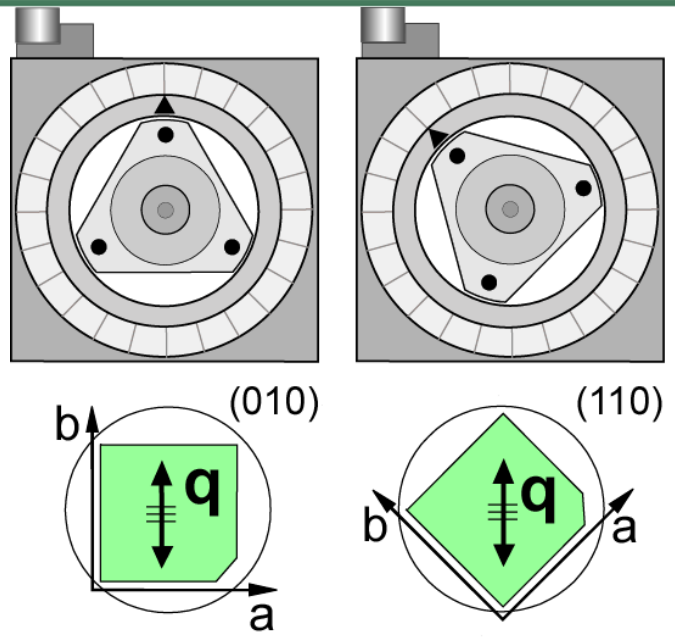

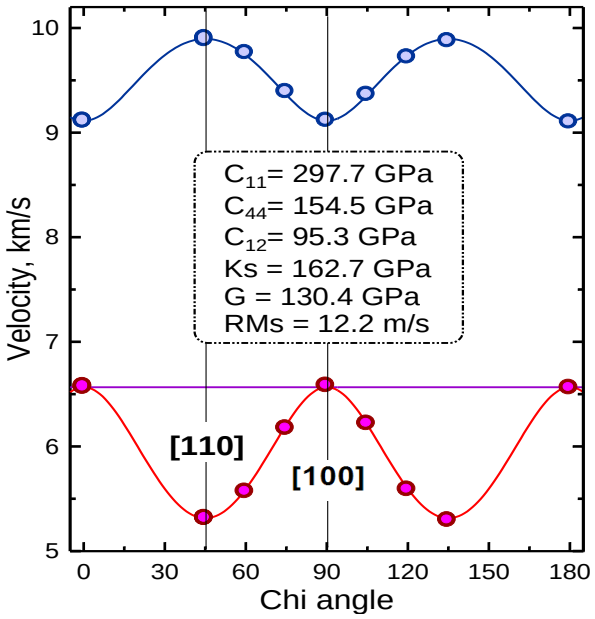

Courtesy to S. V. Sinogeikin

Measured acoustic velocities of Lawsonite as a function of crystallographic direction projected on the *a*-*b*, *b*-*c*, and *a*-*c* planes.

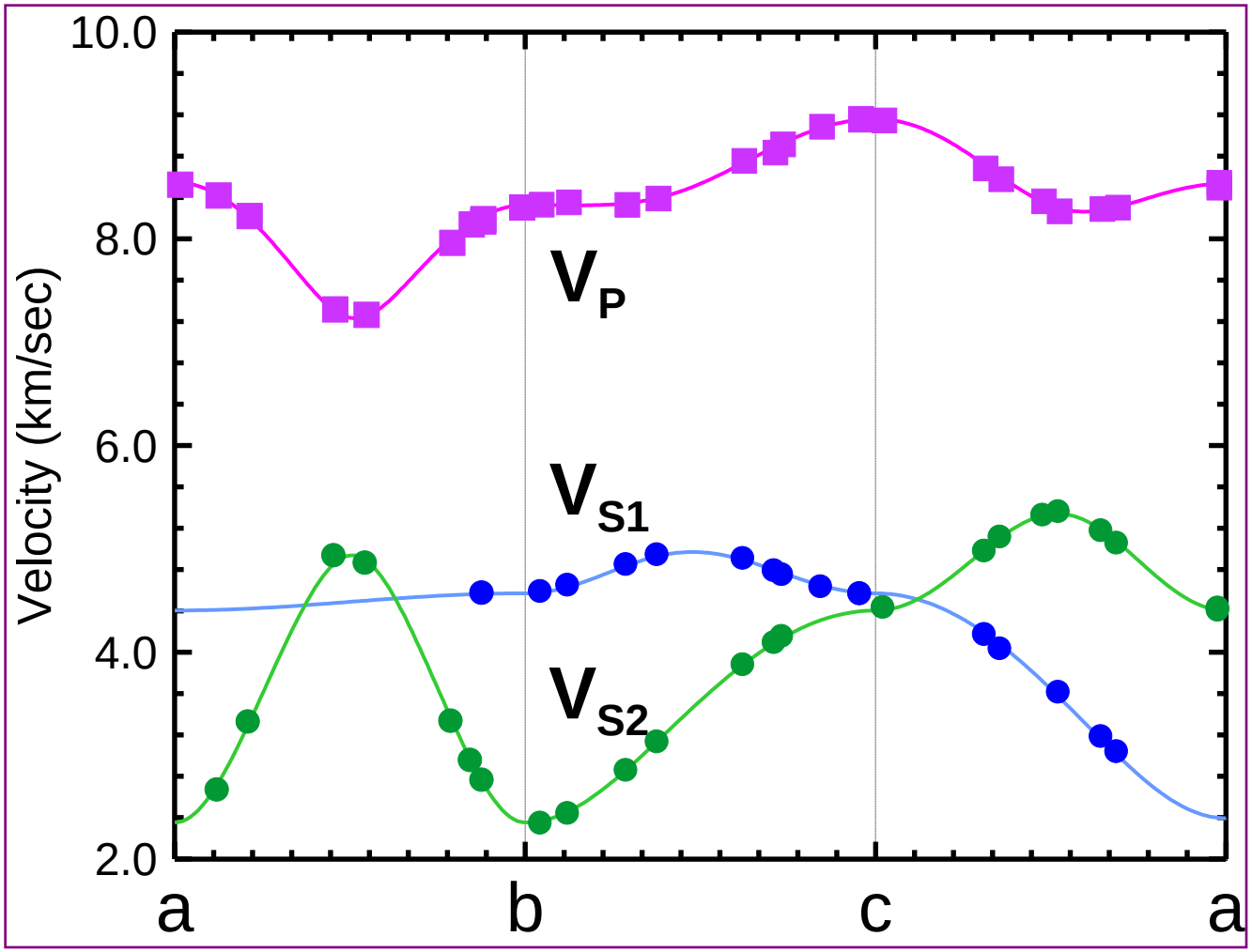

Solid lines are calculated from the best fit elastic constants.

Courtesy to S. V. Sinogeikin

Surface Brillouin Scattering of GaAs

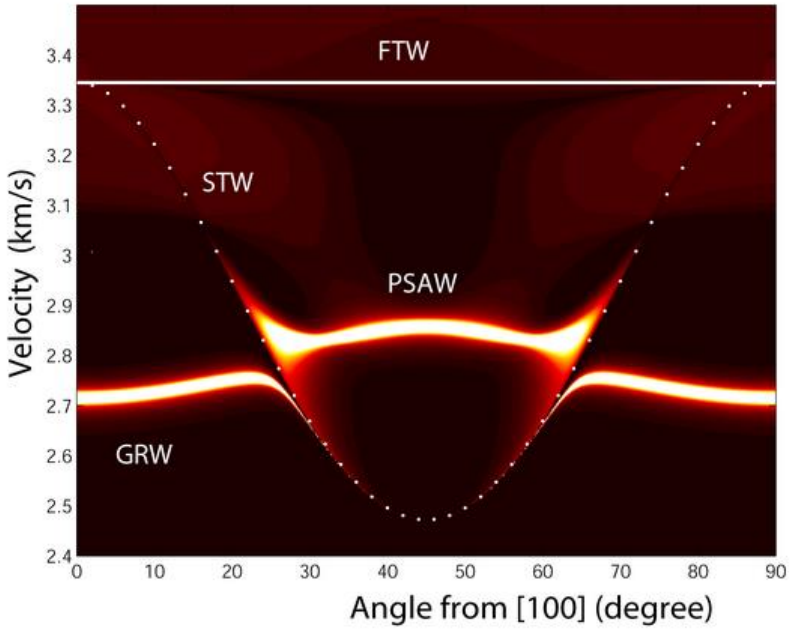

Green's function $G_{33}(\mathbf{k}_{\|},\omega)$ simulation of the SAW dispersion on the (001) surface of GaAs.

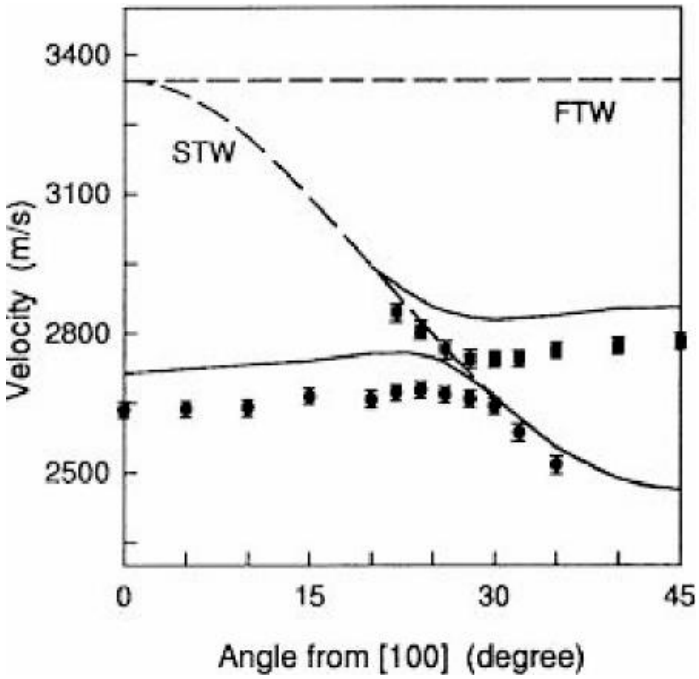

Angular dependence of the measured GSW and PSW velocities on (001) GaAs. Experimental data for GSW and PSW are denoted by circles and squares, respectively. Solid curves represent the theoretical surface wave velocities, while the FTW and STW bulk wave velocities are shown as dashed curves (From Kuok et al., *J. Appl. Phys.* 89 (12), 7899, 2001 With permission).

Surface Brillouin Scattering of GaAs

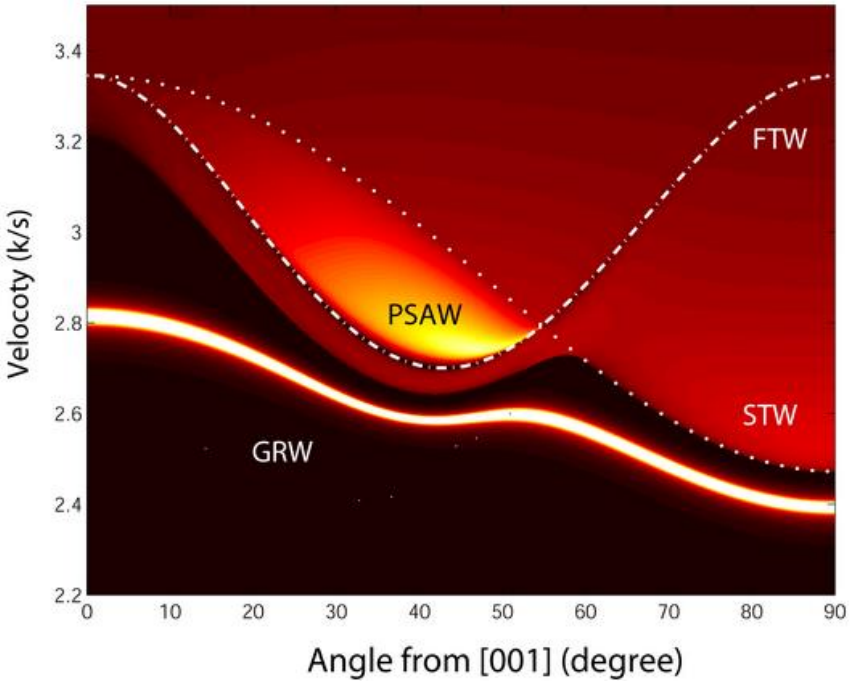

Green's function $G_{33}(\mathbf{k}_{\|},\omega)$ simulation of the SAW dispersion on the (110) surface of GaAs.

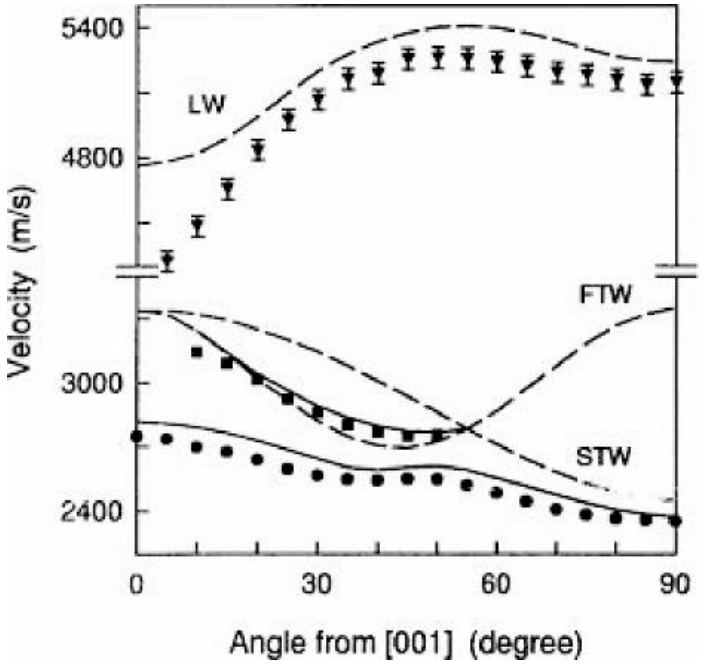

Angular dependence of the surface acoustic wave velocities on (110) GaAs. The experimental data for GSW, PSW, and HFPSW are represented by circles, squares, and inverted triangles, respectively. Solid curves represent theoretical surface wave velocities, while theoretical bulk wave velocities are shown as dashed curves.(From Kuok et al., *J. Appl. Phys.* 89 (12), 7899, 2001 With permission).

Bulk Brillouin scattering in Platelet Geometry

- Acoustic waves present in a solid due to thermal motion of atoms
- Laser light interacts with phonons (or density / refractive index fluctuations) and is scattered with Doppler shifted frequency $\Delta\omega$
- In symmetric platelet geometry the Brillouin shift is directly proportional to acoustic velocity

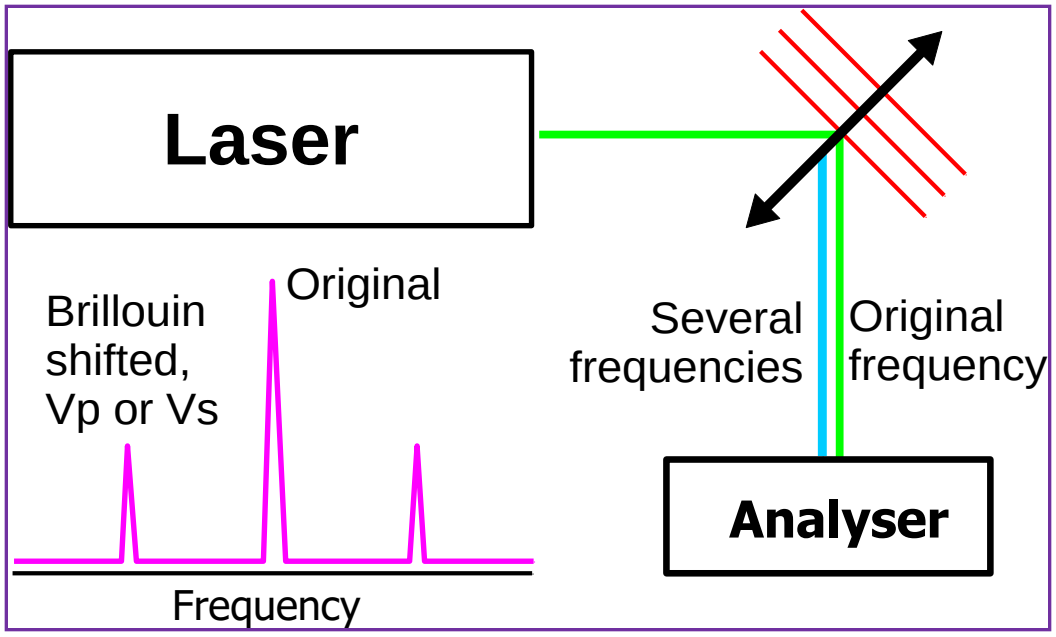

$$V = \frac{\lambda_o \Delta f}{2 \sin \theta}$$

S. V. Sinogeikin, J. D. Bass, V.B. Prakapenka et al, Rev. Sci. Instrum. 77, 103905 2006

Brillouin Scattering at the Argonne National Laboratory

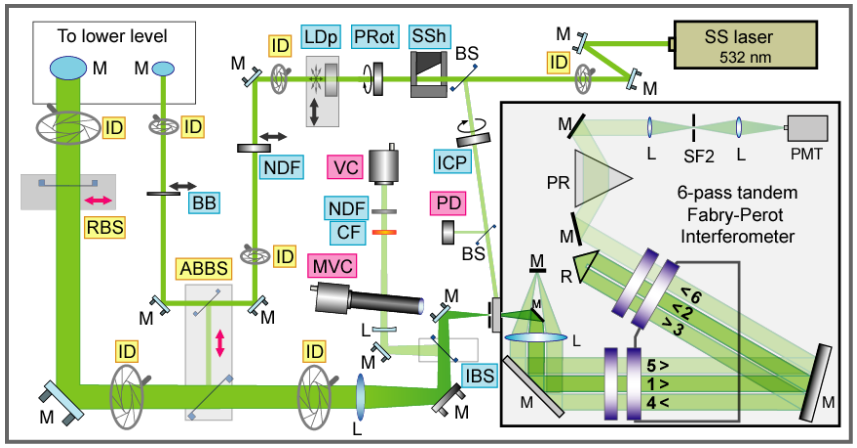

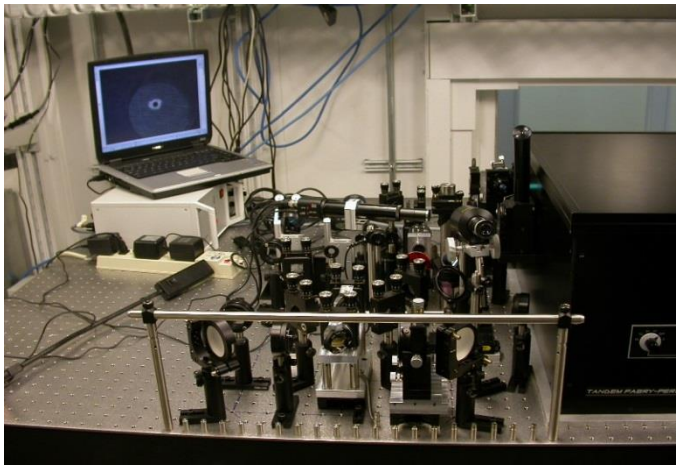

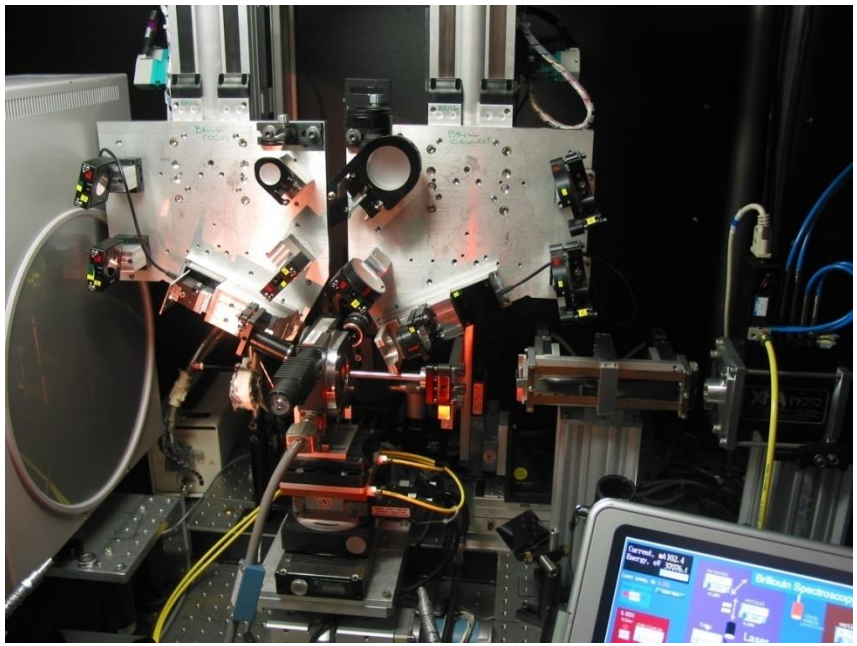

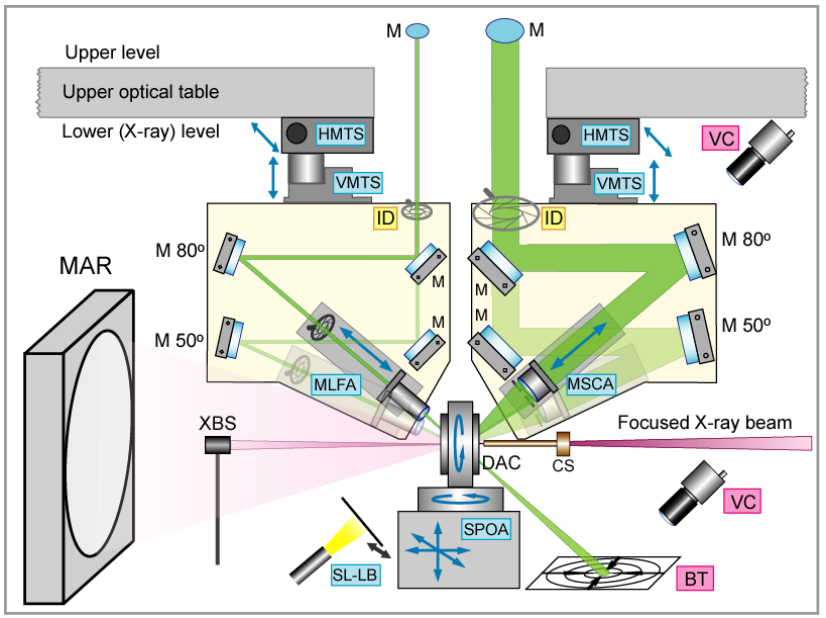

S. V. Sinogeikin, J. D. Bass, V.B. Prakapenka, *Rev. Sci. Instrum*. 77, 103905 2006

Brillouin measurements in DAC - samples

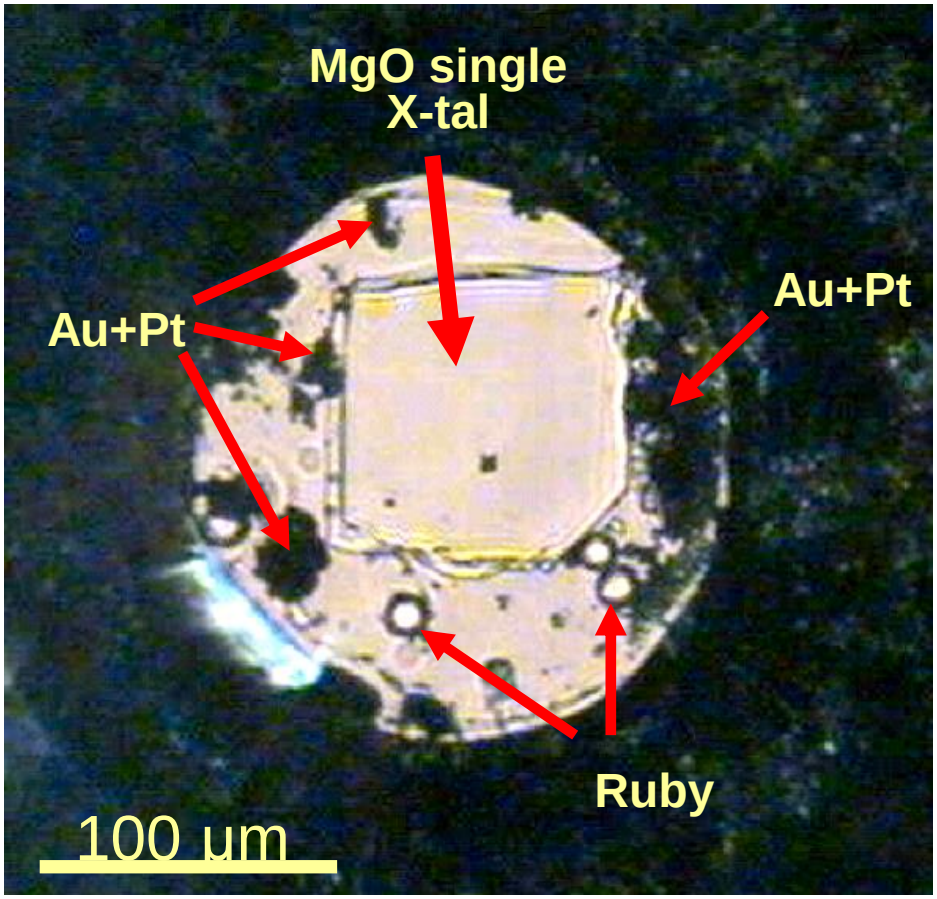

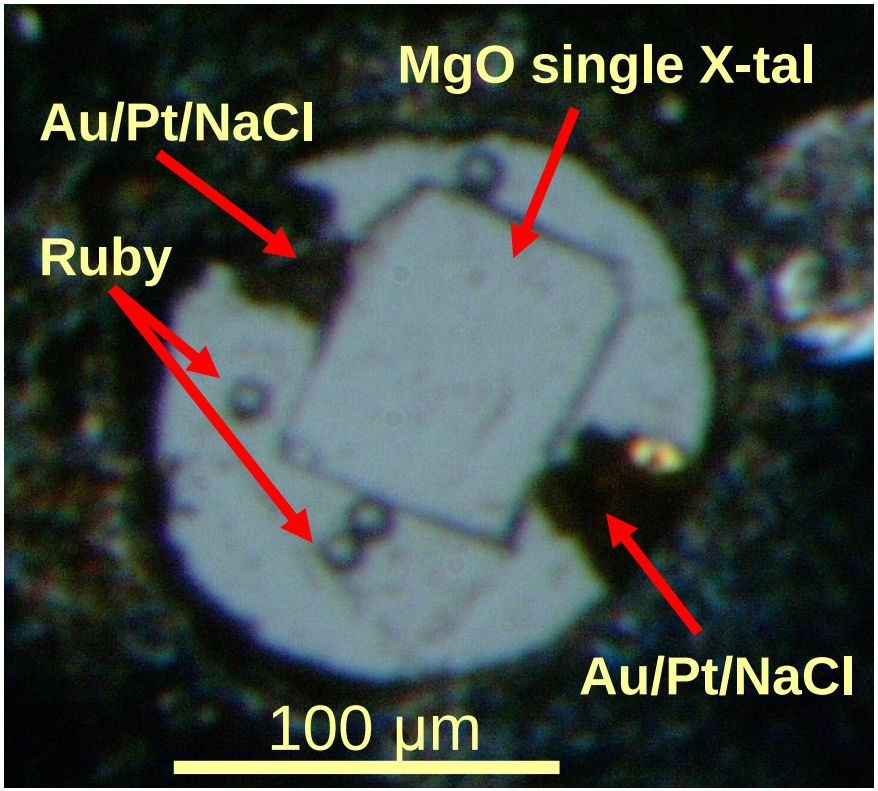

Typical DAC load for x-ray / Brillouin measurements

Courtesy to S. V. Sinogeikin

XRD and BS of single crystal MgO in [100] direction in the DAC at 4 GPa

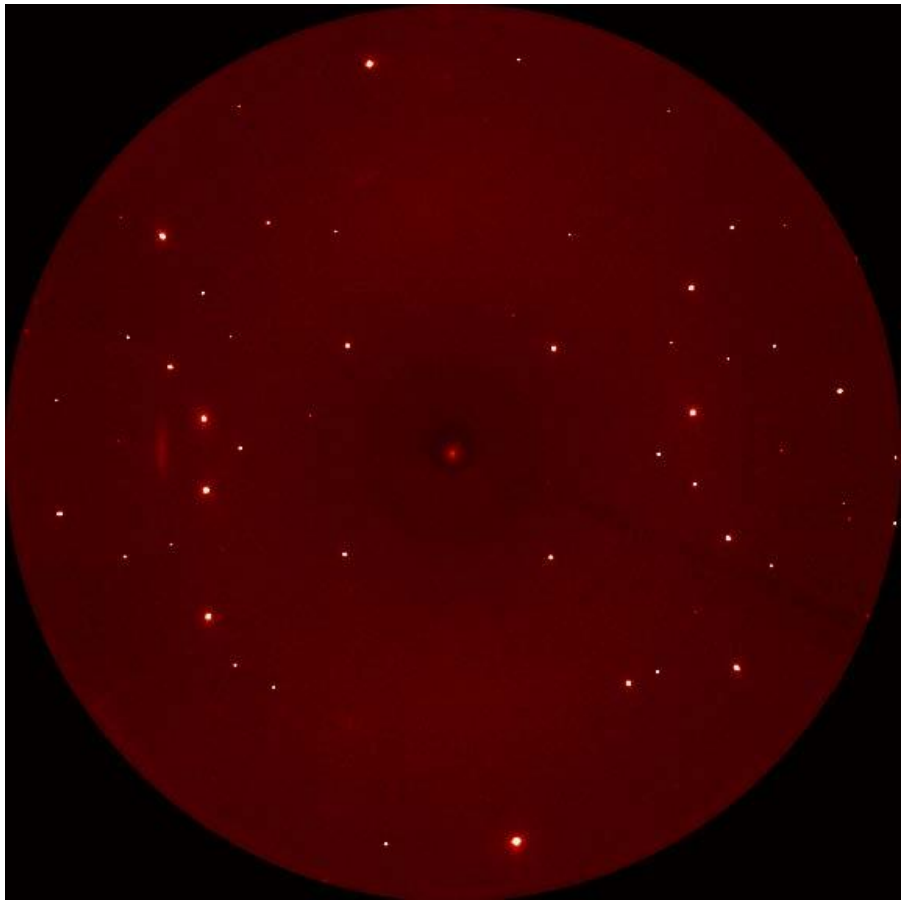

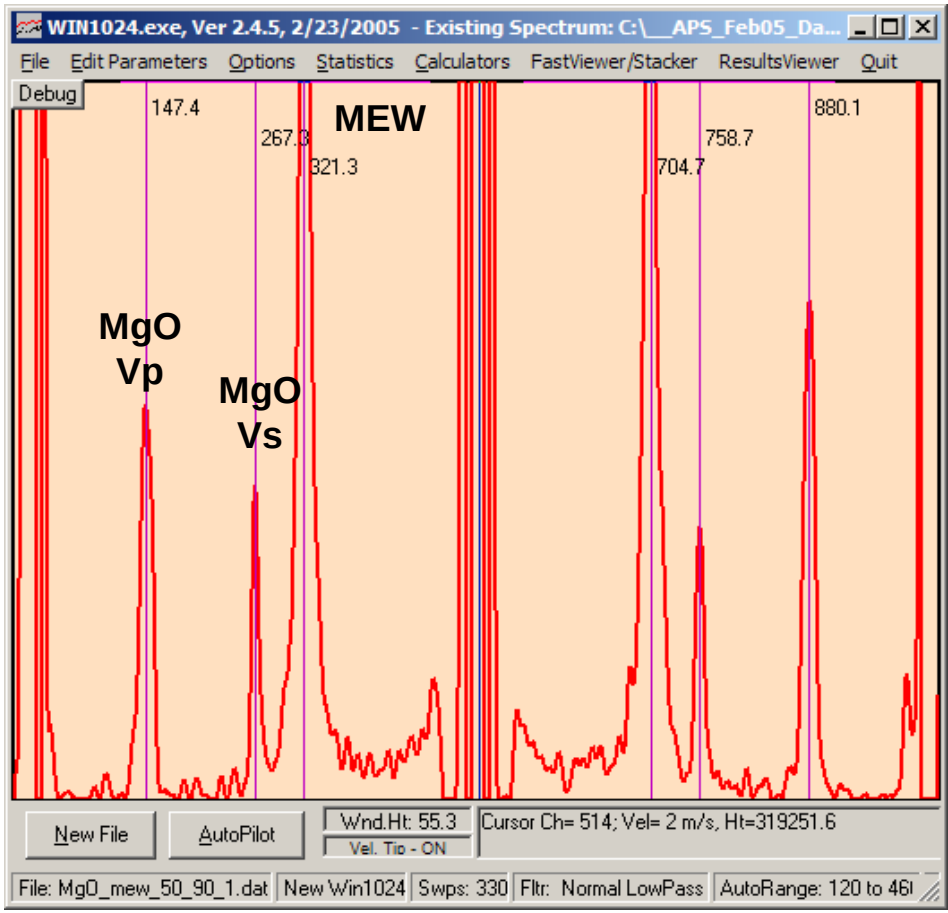

S. V. Sinogeikin, J. D. Bass, V.B. Prakapenka, Rev. Sci. Instrum. 77, 103905 2006

XRD and BS of MgO in [100] direction in the DAC at 8 GPa and ~800 K

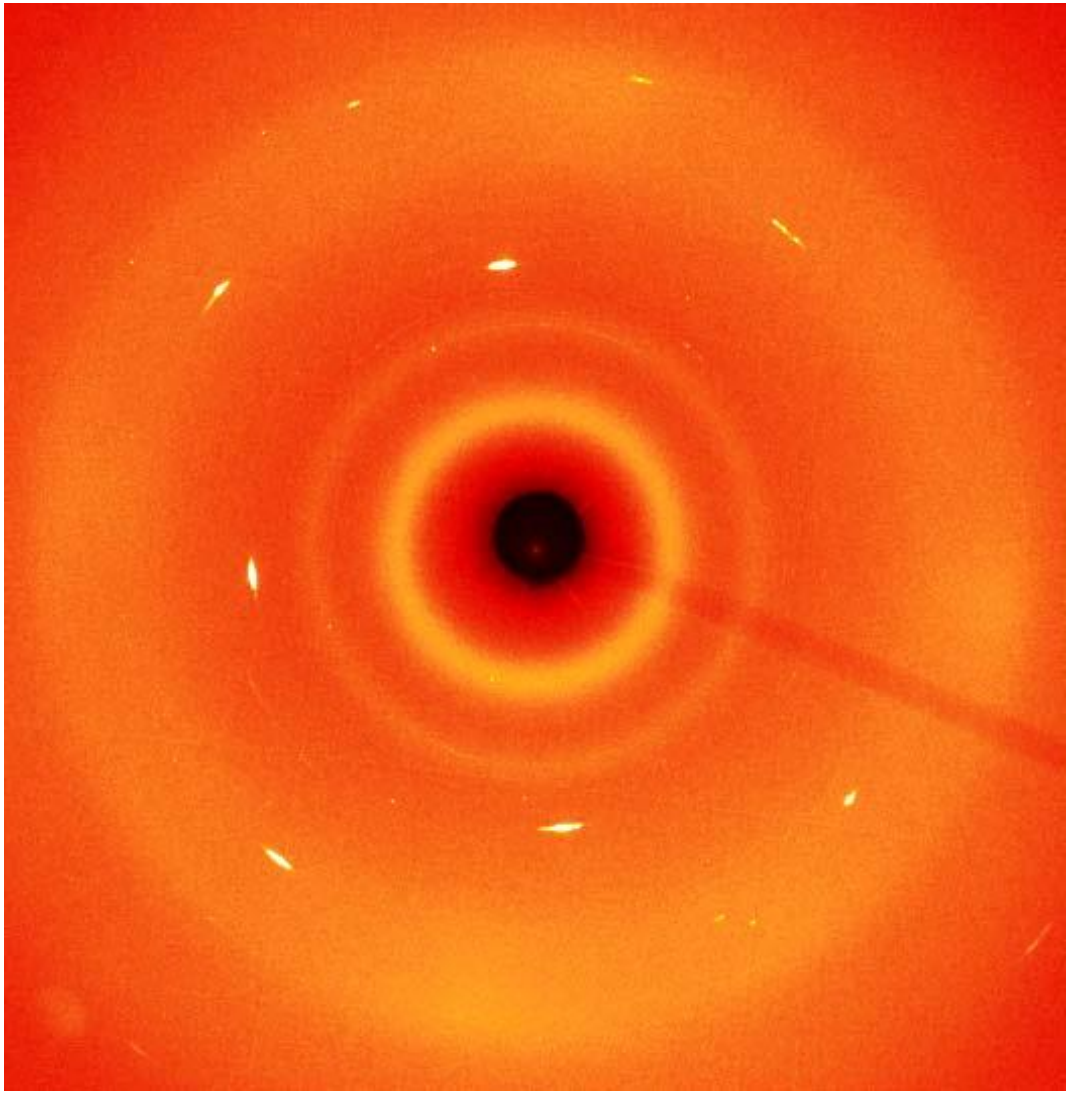

Ar pressure medium is melted

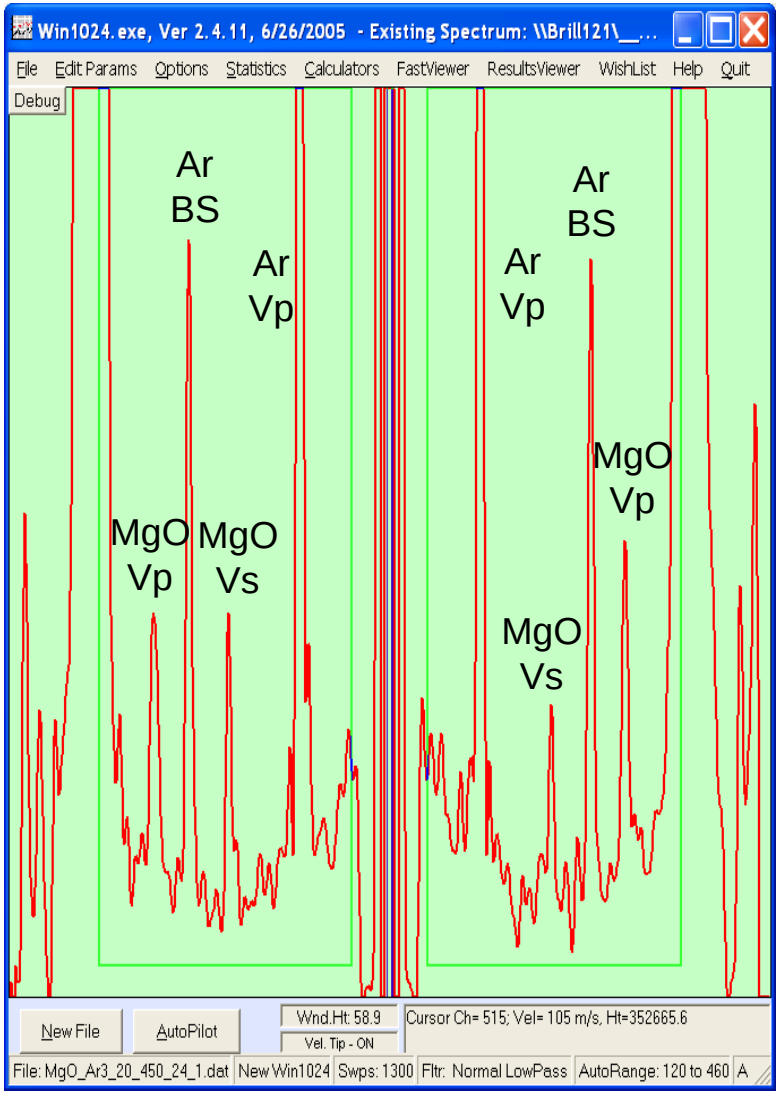

collection time ~10 minutes

XRD and BS measurements on single crystal (Mg,Fe)O at 82 GPa

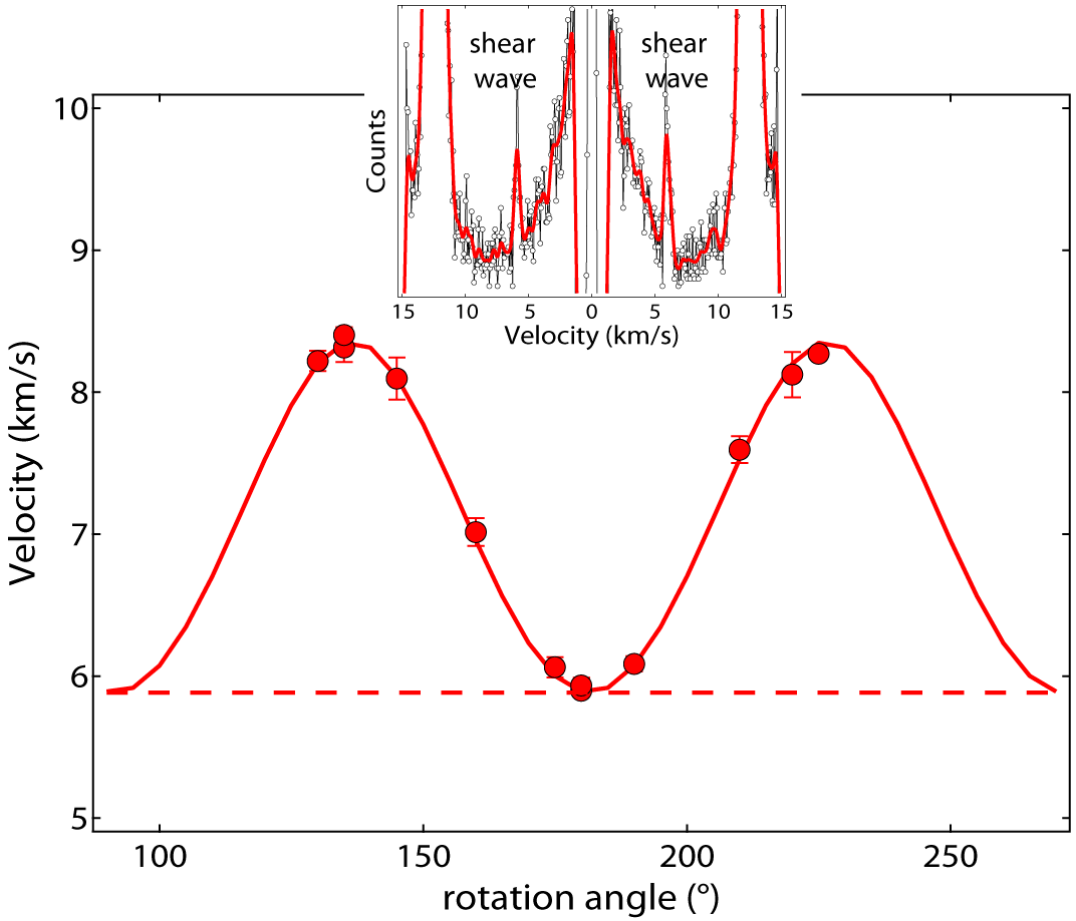

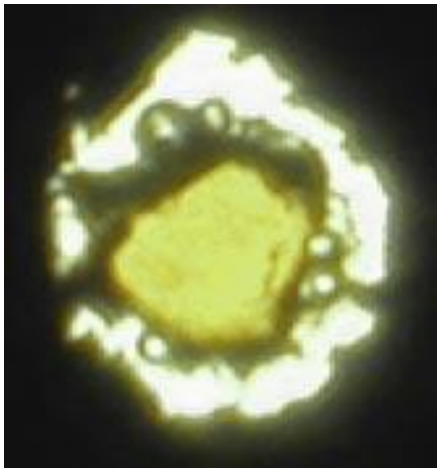

50um

Marquardt, Speziale, et al, 2009

XRD and BS of MgO in [100] direction in the DAC at 8 GPa and ~800 K

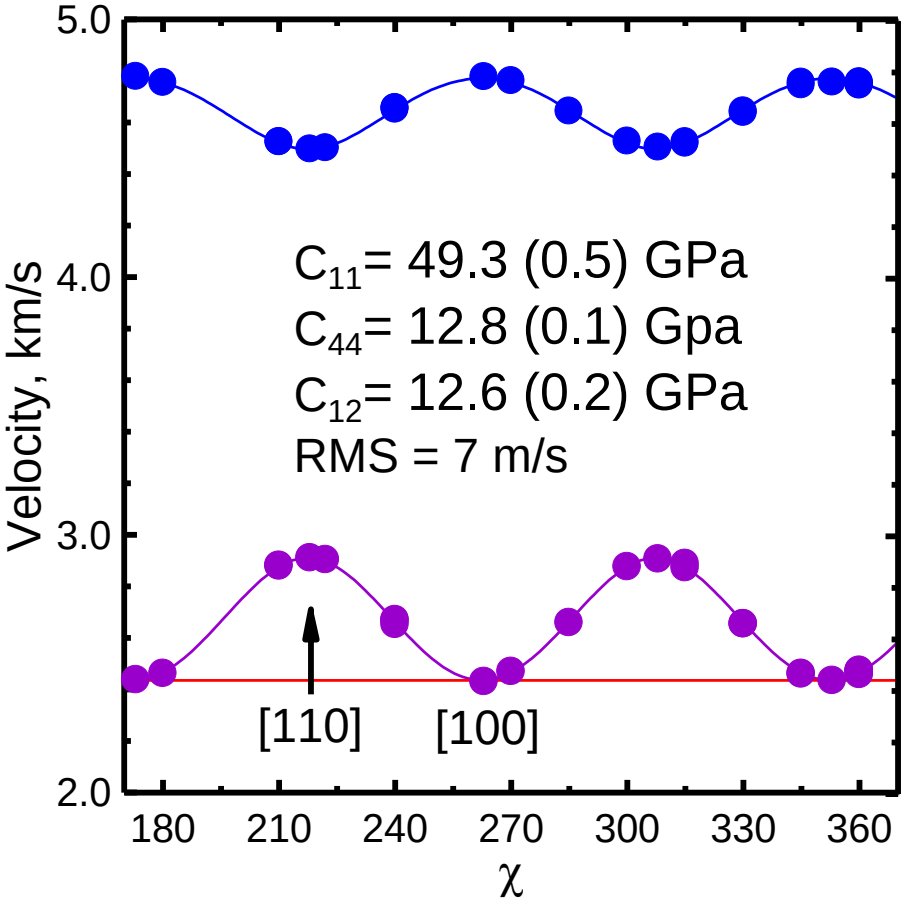

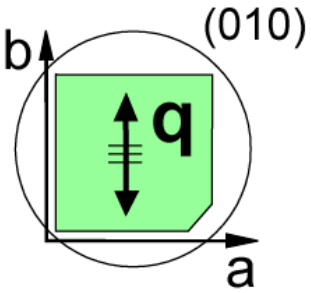

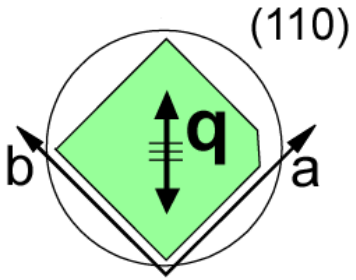

S. V. Sinogeikin, J. D. Bass, V.B. Prakapenka et al, Rev. Sci. Instrum. 77, 103905 2006

Sound velocity of $MgSiO_3$ perovskite to Mbar pressure

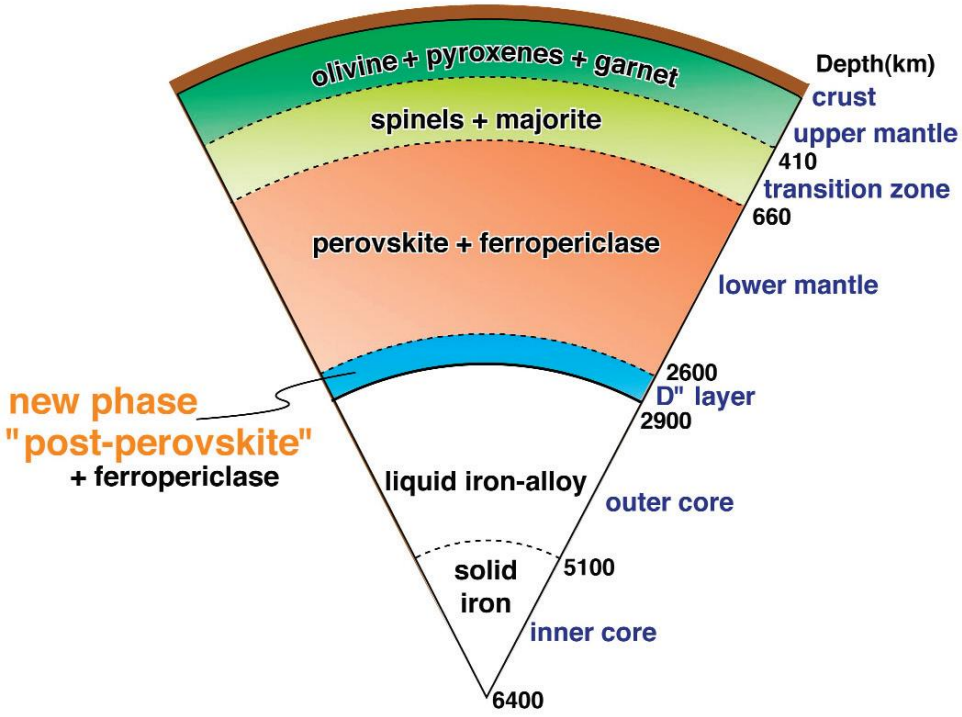

Simplified cross-section of the Earth. The main constituent minerals in the mantle change from olivine + pyroxenes + garnet (or Al-rich spinel) in the upper mantle, to spinels + majorite in the transition zone, to perovskite + ferropericlase in the lower mantle, and to post-perovskite + ferropericlase in the D” layer. The boundaries between the layers are characterized by seismic-wave discontinuities.

Phase Transformations in the Mantle

Bernal was the first to propose that rapid increases in seismic velocity in the mantle might be due to phase transformations rather than a change in composition. Experiments in the mid-1960s showed that the olivine component of *peridotite* undergoes successive pressure-dependent transformations to the *spinel* structure (*ringwoodite*), and ultimately breaks down to form $(Mg,Fe)SiO_3$ *perovskite* plus (Mg,Fe)O :

$(Mg,Fe)_2SiO_4 = (Mg,Fe)_2SiO_4$ Pressure, 13-14 GPa; depth, 410 km

Olivine *Wadsleyite*

$(Mg,Fe)_2SiO_4 = (Mg,Fe)_2SiO_4$ Pressure, 18 GPa; depth, 520 km

Wadsleyite *Ringwoodite*

$(Mg,Fe)_2SiO_4 = (Mg,Fe)SiO_3 + (Mg,Fe)O$ Pressure, 23 GPa; depth, 660 km

Ringwoodite *Perovskite* *Magnesiowustite*

Sound velocity of $MgSiO_3$ perovskite to Mbar pressure

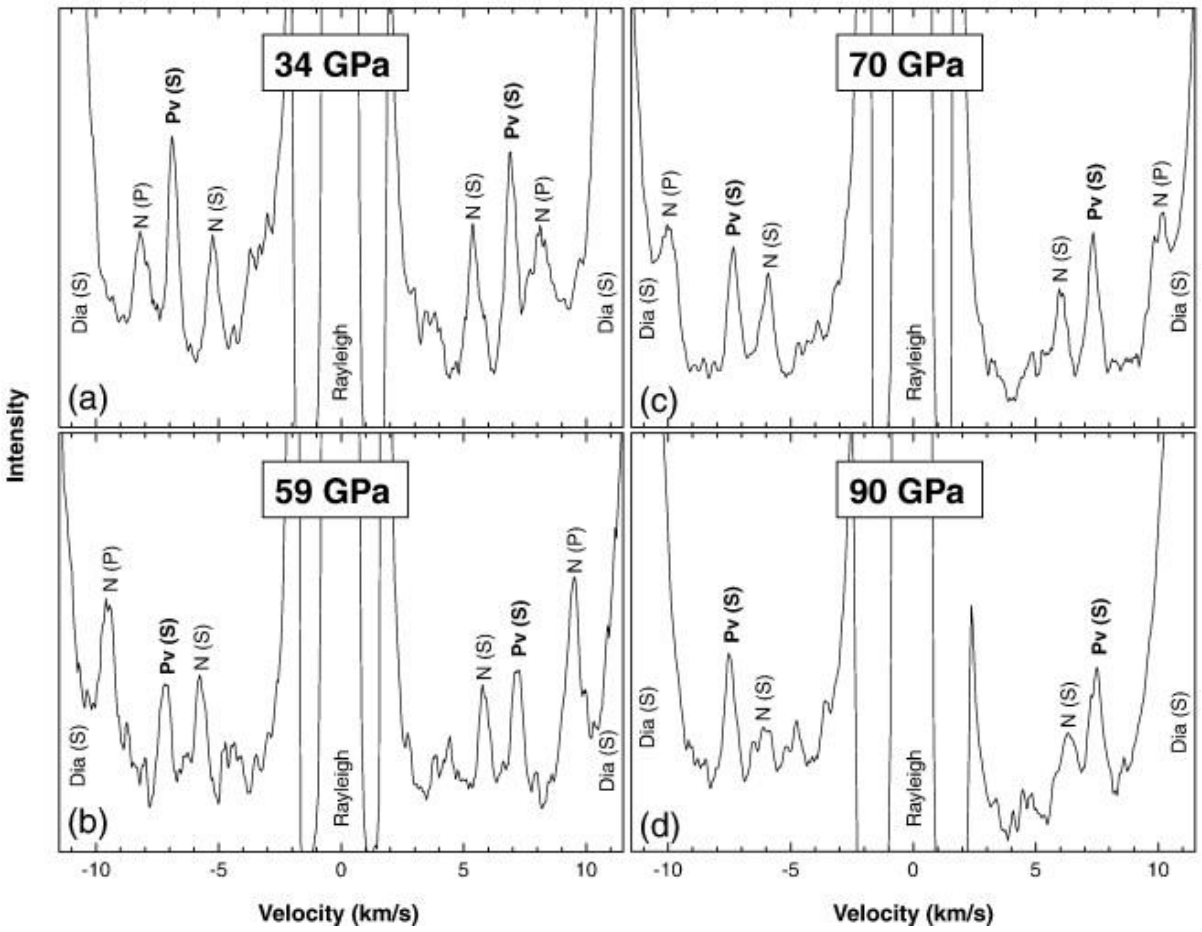

Representative Brillouin spectra at pressures of 34 (a), 59 (b), 70 (c) and 90 GPa (d). Pv, $MgSiO_3$ perovskite; N, NaCl pressure medium; Dia, diamond; (S), shear acoustic mode; (P), longitudinal acoustic mode.

(M. Murakami, S. Sinogeikin, H. Hellwig, J. D. Bass J. Li. *Earth Plant Scie Lett.* 2007).

Sound velocity of $MgSiO_3$ post-perovskite

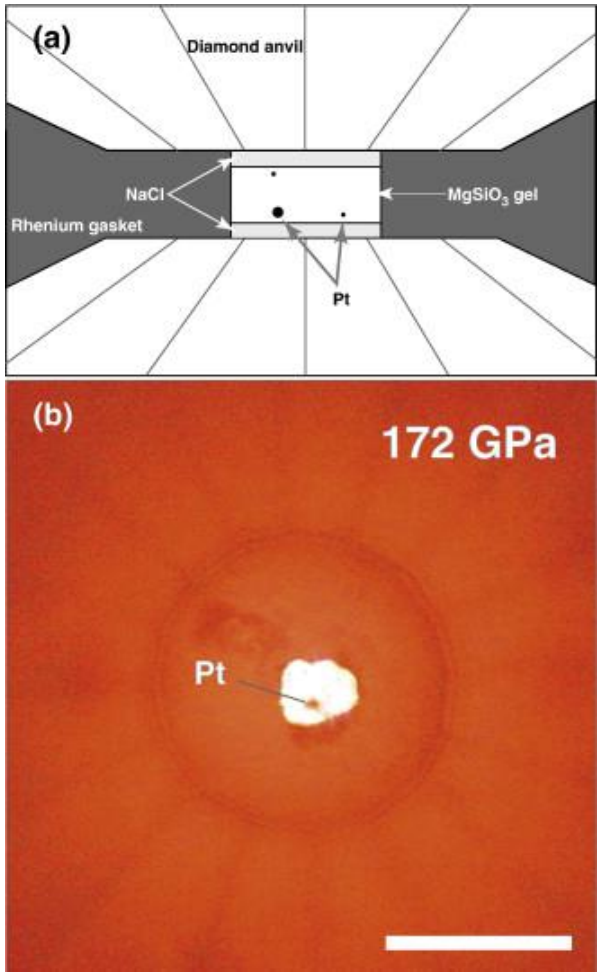

M. Murakami *et al.*, *Earth Planet. Sci. Lett.* **259** 18 2007

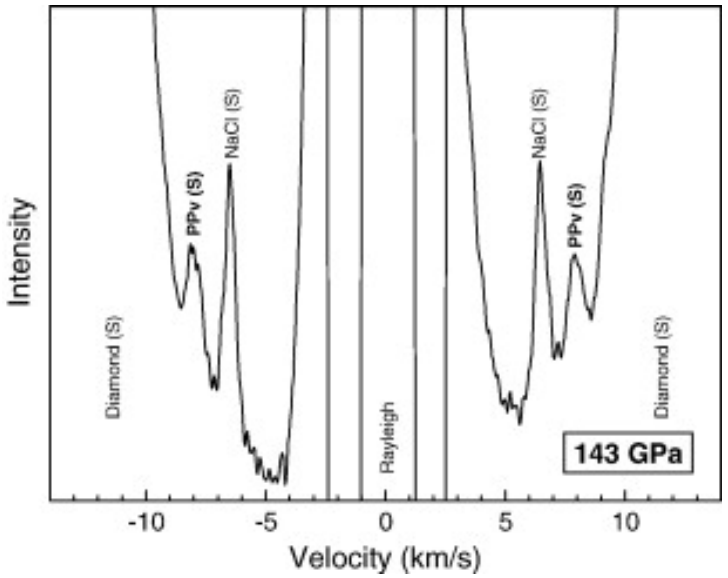

Representative high pressure Brillouin spectrum at 143 GPa. PPv, $MgSiO_3$ post-perovskite phase; (S), shear acoustic mode (V_S).

Arrangement of the sample in the diamond anvil cell for high pressure Brillouin scattering. (a) Schematic cross section of the diamond anvil cell assembly before laser heating. (b) Microscopic image of the sample at 172 GPa after laser heating as viewed through the diamond anvil. Scale bar indicates 100 μm.

Sound velocity of $MgSiO_3$ perovskite to Mbar pressure

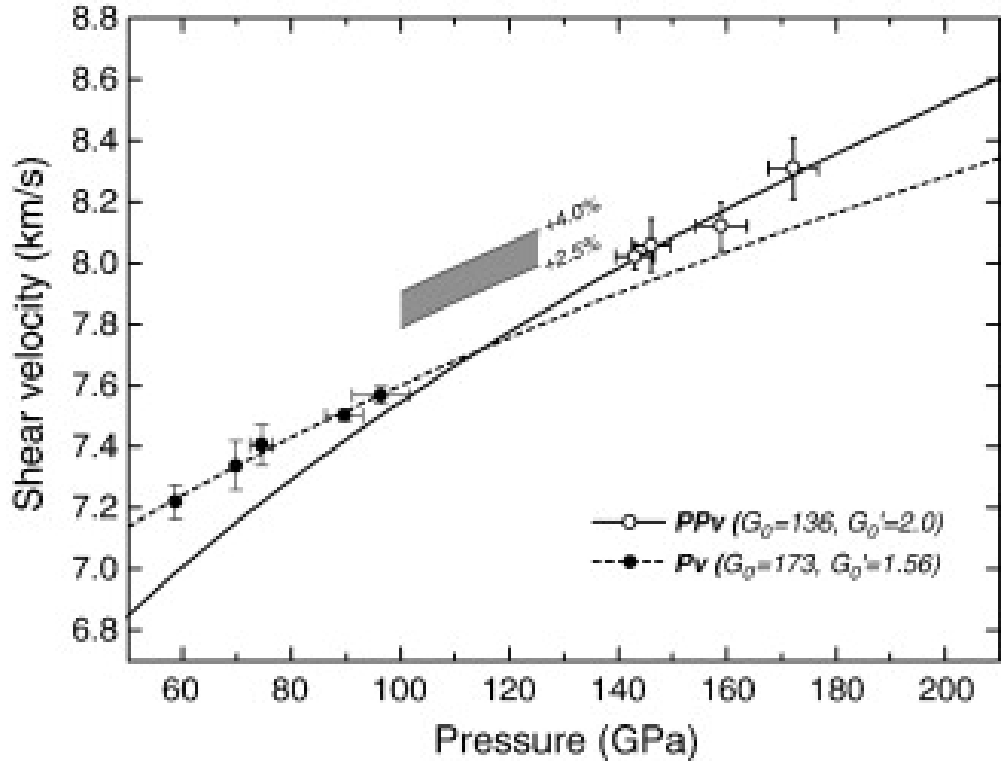

Shear wave velocities of $MgSiO_3$ perovskite and post-perovskite phase as a function of pressure at 300 K. Open circles show the data of post-perovskite phase in the present study, and filled circles those of perovskite from M. Murakami *et al.*, : *Earth Planet. Sci. Lett.* **259** 18 2007. Third-order Eulerian finite-strain fits are shown by solid line for post-perovskite and dashed line for perovskite, respectively. The shaded area indicates the shear velocity jump of 2.5–4.0% (Wysession et al., 1998) from that of perovskite from 100 to 125 GPa.

D-layer

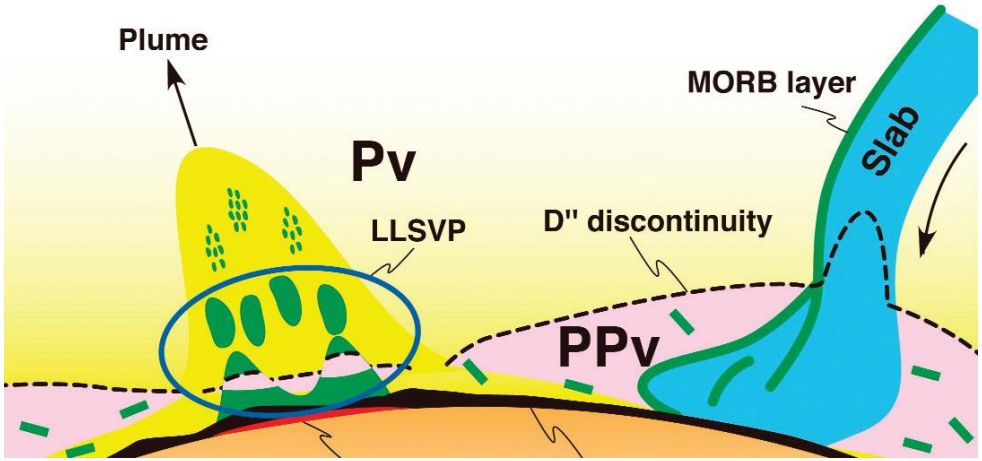

Cartoon scenario for the D” region. The D” seismic discontinuity is caused by the perovskite (Pv) to post-perovskite (PPv) phase transition. Post-perovskite may transform back to perovskite in the bottom thermal boundary layer with a steep temperature gradient. The large low-shear-velocity provinces (LLSVP) underneath upwellings (forming plumes) possibly represent large accumulations of dense mid-oceanic ridge basalt (MORB)-enriched materials. The solid residue formed by partial melting in the ULVZ might also be involved in upwelling plumes.

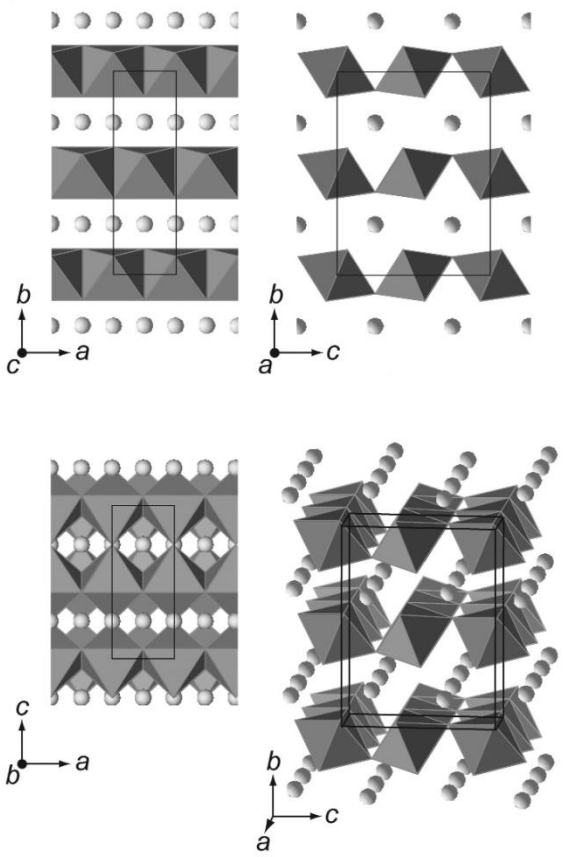

Crystal structure of the post-perovskite phase projected along (A) (001), (B) (100), and (C) (010) directions, and (D) a stereoscopic view showing the layer-stacking structure (after Murakami et al. 2004).

Brillouin spectroscopy

Advantages:

- direct measurements of acoustic velocities
- nondestructive optical spectroscopy
- very small samples (down to 10-20 μm)
- from single crystal to non-crystalline materials
- measurements at P-T conditions of the Lower Mantle

Disadvantages:

- complicated optical system
- transparent and translucent samples
- elastic moduli only for known density

Shear: $\mu=\rho V^2_S$

Bulk: $K_S=\rho V^2_P - 4/3\ \mu$

Single-crystal: $C_{11} = \rho V_p^2{}_{(100)}$

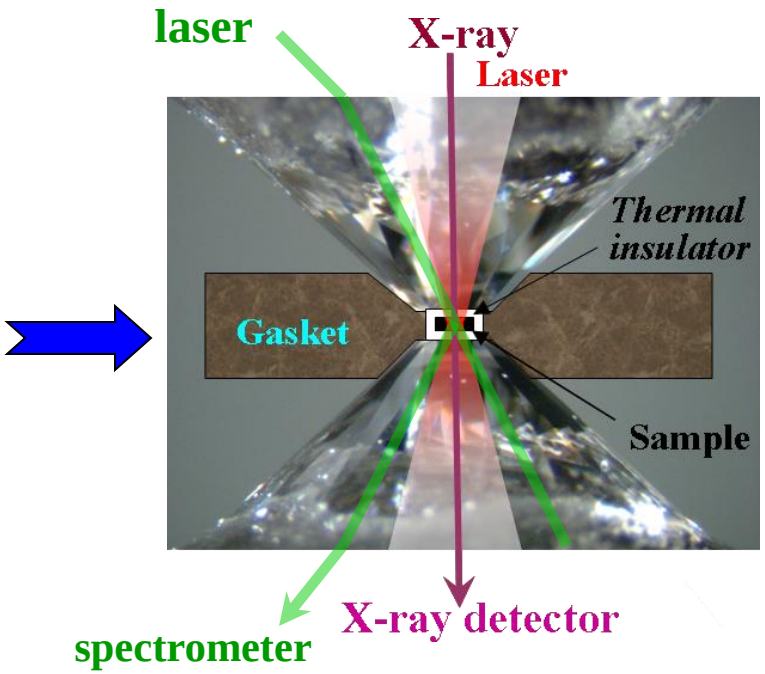

S. V. Sinogeikin, J. D. Bass, V.B. Prakapenka, Rev. Sci. Instrum. 77, 103905 2006

Home Reading

1. M. G. Beghi, A. G. Every, and P. V. Zinin. “Brillouin Scattering Measurement of SAW Velocities for Determining Near-Surface Elastic Properties”, in T. Kundu ed., *Ultrasonic Nondestructive Evaluation: Engineering and Biological Material Characterization*. CRC Press, Boca Raton, chapter 10, 581-651 (2004).

2. P. V. Zinin, and M. H. Manghnani. “Elasticity Characterization of Covalent (B-C-N) Hard Materials and Films by Brillouin scattering”, in G. Amarendra, Raj, B. and M. H. Manghnani eds. *Recent Advances in Materials Characterization*. CRC Press, London, 184-211 (2006)

3. S. Sinogeikin, J. Bass, V. Prakapenka, D. Lakshtanov, G. Shen, C. Valle, M. Rivers, "Brillouin spectrometer interfaced with synchrotron radiation for simultaneous x-ray density and acoustic velocity measurements," *Rev. Sci. Instrum*. 77, 103905-1-103905-11 (2006).

4. Every, A. G., “The Elastic Properties of Solids: Static and Dynamic Principles, in Handbook of Elastic Properties of Solids, Liquids, and Gases”. Volume I: *Dynamic Methods for Measuring the Elastic Properties of Solids*, Levy, M., Bass, H., Stern, R., and Keppens, V. Academic Press, New York, 2001, pp. 3-36.